

Multifunctional Bisalkynylplatinum(II) Bipyridine Complexes with Rodamine-Like Ligands

Featuring Near-Infrared Phosphorescence and Delayed Fluorescence

Shunan Zhao,^{a,b} Jianfeng Song^b and Keith Man-Chung Wong^{*b}

^a School of Chemistry and Chemical Engineering, Harbin Institute of Technology, Harbin 15001, China.

^b Department of Chemistry, Southern University of Science and Technology, No. 1088 Xueyuan Blvd., Shenzhen, 518055, P.R. China.

E-mail: keithwongmc@sustech.edu.cn

Electronic Supplementary Information

Experimental

Instruments

NMR spectra were recorded on a Bruker AVANCE 400 (^1H NMR for 400 MHz) Fourier-transform NMR spectrometer and a Bruker AVANCE 500 (^1H NMR for 500 MHz) Fourier-transform NMR spectrometer with chemical shifts reported relative to tetramethylsilane, $(\text{CH}_3)_4\text{Si}$. The UV-visible absorption spectra were taken on Cary 60 UV-vis spectrophotometer. Steady state emission spectra at room temperature were recorded on an Edinburgh Instruments FS5 Fluorescence Spectrometer. Transient absorption and time-resolved emission spectra at room temperature were measured on Edinburgh Instruments PL920 with 355 nm and 532 nm pump laser generator. The upconversion quantum yields (Φ_{UC}) were determined with Rhodamine B as the quantum-yield standard ($\Phi_F = 0.4$ in deaerated CH_3CN) following the same methods in reported works.^{3,4} Quartz cuvettes (path-length = 1 cm) was used in all spectrophotometric and fluorometric measurements. High resolution mass spectra were performed on Orbitrap Fusion™ Tribrid™ Mass spectroscopy. Elemental analyses of complexes were performed on an Elementar Vario EL cube elemental analyzer.

The singlet oxygen ($^1\text{O}_2$) emission measurements were carried out on an Edinburgh instrument FLS 980. An 850 nm filter was inserted between the sample and the detector to inhibit the high-order diffraction from the visible region. Open-form of **1–6** and Rose bengal were dissolved in MeCN. The absorption at 514.5 nm which was used as the excitation wavelength was adjusted to around 0.38 for all compounds. The singlet oxygen quantum yield was calculated by comparing the $^1\text{O}_2$ emission spectrum of Rose Bengal under excitation at 514.5 nm ($\Phi_\Delta = 45\%$ in MeCN).⁵

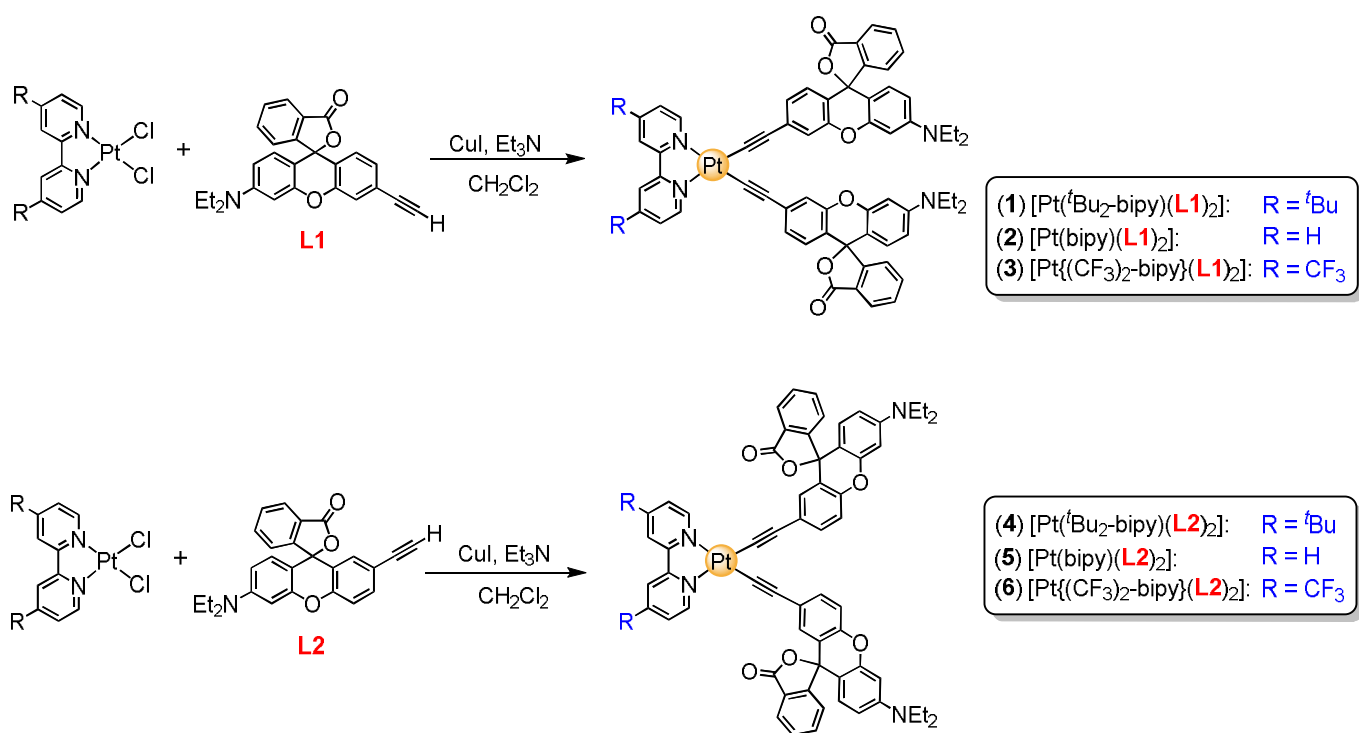
Materials and Reagents.

All the solvents for synthesis were of analytical grade. Acetonitrile for analysis was of spectroscopy grade. 3-(Diethylamino)phenol, phthalic anhydride, 4-bromophenol, 3-bromophenol,

potassium tetrachloroplatinate(II), 2,2'-bipyridine, 4,4'-di-tert-butyl-2,2'-bipyridine, 4,4'-bis(trifluoromethyl)-2,2'-bipyridine, trimethylsilylacetylene, cuprous iodide, tetrabutylammonium fluoride were purchased from Aldrich Chemical Co. $[\text{Pt}(\text{R}_2\text{-bpy})\text{Cl}_2]$ were synthesized according to the reported procedures.^{S1} Rhodyne ligands **L1** and **L2** were prepared by following the same methods from our previous work.^{S2}

Synthesis

Complexes **1–6** were synthesized according to the modification of reported procedures.^{S1} The synthetic methods for complexes **1–6** were similar. Reaction of complex $[\text{Pt}(\text{R}_2\text{-bpy})\text{Cl}_2]$ with **L1** or **L2** ligands at room temperature in the presence of Et_3N and catalytic amount of CuI afforded the target complexes **1–6** (Scheme S1).



Scheme S1. The synthetic routes of complexes **1–6**.

Synthesis of complex 1 $[\text{Pt}(^t\text{Bu}_2\text{-bipy})(\text{L1})_2]$. $[\text{Pt}(^t\text{Bu}_2\text{-bipy})\text{Cl}_2]$ (421 mg, 1.0 mmol), **L1** (395 mg,

1.0 mmol) and catalytic amount of Cul were added into a Schlenk flask under the protection of nitrogen atmosphere. Distilled and dried dichloromethane (30 ml), and triethylamine (1 ml) were transferred into the flask. After stirring about 20 h, all solvent was removed and dark yellow residual was obtained. Through column chromatography with silica gel by suing dichloromethane:acetone (10:1) as the eluent, yellow powder was collected after removal of solvent. The target complex was subsequently recrystallized by diffusion of diethyl ether vapor into acetonitrile solution of **1**. Yield: 220 mg, 17.6 %. ¹H NMR (400 MHz, DMSO) δ 9.64 (d, *J* = 6.0 Hz, 2H), 8.00 (d, *J* = 7.5 Hz, 2H), 7.96 (d, *J* = 1.7 Hz, 2H), 7.65 (dt, *J* = 7.5, 3.8 Hz, 2H), 7.58 (dd, *J* = 8.8, 4.7 Hz, 4H), 7.4 (d, *J* = 1.5 Hz, 2H), 7.21 (d, *J* = 7.6 Hz, 2H), 7.12 (dd, *J* = 8.8, 1.5 Hz, 2H), 6.57 (dd, *J* = 16.4, 8.5 Hz, 4H), 6.46 (d, *J* = 2.5 Hz, 2H), 6.33 (dd, *J* = 8.9, 2.6 Hz, 2H), 3.36 (q, *J* = 7.0 Hz, 8H), 1.42 (s, 18H), 1.17 (t, *J* = 7.0 Hz, 12H). ¹³C NMR (100 MHz, DMSO): δ 207.01, 169.24, 164.81, 156.25, 152.85, 152.71, 151.34, 150.36, 149.78, 136.08, 130.81, 130.59, 129.17, 128.03, 127.59, 126.76, 125.54, 125.09, 124.58, 121.75, 119.02, 116.83, 109.15, 104.78, 100.47, 97.40, 94.35, 83.84, 60.23, 44.27, 36.46, 31.17, 30.33, 21.24, 14.56, 12.80. HRMS (ESI) for [C₇₀H₆₆N₄O₆Pt]²⁺: calcd 626.73096, Found 626.73118. Elemental analysis calcd (%) for C₇₀H₆₄N₄O₆Pt•CH₃CN: C, 66.86; H, 5.22; N, 5.41; found: C, 66.75; H, 5.18; N, 5.39.

Synthesis of complex 2 [Pt(bpy)(L1)₂]. The synthetic procedure was similar to that of complex **1** except that [Pt(bpy)Cl₂] was used instead of [Pt(^tBu₂-bpy)Cl₂]. Yield: 196 mg, 16.6%. ¹H NMR (400 MHz, DMSO) δ 9.39 (d, *J* = 5.0 Hz, 2H), 8.69 (d, *J* = 8.2 Hz, 2H), 8.41 (t, *J* = 7.7 Hz, 2H), 8.01 (d, *J* = 7.5 Hz, 2H), 7.92-7.86 (m, 2H), 7.80 (t, *J* = 7.4 Hz, 2H), 7.72 (t, *J* = 7.4 Hz, 2H), 7.4 (s, 2H), 7.31 (d, *J* = 7.6 Hz, 2H), 7.15 (d, *J* = 8.1 Hz, 2H), 6.63(d, *J* = 8.2 Hz, 2H), 6.51-6.45 (m, 6H), 3.40-3.32 (m, 8H), 1.09 (t, *J* = 6.9 Hz, 12H). ¹³C NMR (100 MHz, DMSO) δ 169.22, 156.44, 152.85, 152.69, 151.32, 149.79, 140.82, 136.09, 130.59, 130.12, 129.16, 128.05, 127.66, 125.09, 124.56, 119.16, 117.02, 109.16, 104.76, 97.41, 83.80, 44.26, 31.79, 29.55, 29.49, 29.29, 27.02, 22.56, 12.80. HRMS (ESI) for [C₆₂H₅₀N₄O₆Pt]²⁺: calcd 570.66836, Found 570.66891. Elemental analysis calcd (%) for C₆₂H₄₈N₄O₆Pt•CH₃CN: C, 65.08; H, 4.35; N, 5.93; found: C, 65.19; H, 4.28;

N, 5.77.

Synthesis of complex 3 [Pt{(CF_3)₂-bpy}(L1)₂]. The synthetic procedure was similar to that of complex **1** except that [Pt{(CF_3)₂-bpy}Cl₂] was used instead of [Pt($t\text{Bu}_2$ -bpy)Cl₂]. Yield: 261 mg, 20.5%. ¹H NMR (400 MHz, DMSO) δ 9.78 (d, J = 5.8 Hz, 2H), 9.4 (s, 2H), 8.38 (d, J = 6.0 Hz, 2H), 8.02 (d, J = 7.6 Hz, 2H), 7.82 (t, J = 7.4 Hz, 2H), 7.74 (t, J = 7.4 Hz, 2H), 7.35 (s, 2H), 7.33 (d, J = 7.6 Hz, 2H), 7.11 (d, J = 8.3 Hz, 2H), 6.65 (d, J = 8.2 Hz, 2H), 6.53-6.47 (m, 6H), 3.42-3.34 (m, 8H), 1.11 (t, J = 6.9 Hz, 12H). ¹³C NMR (125 MHz, DMSO) δ 169.21, 157.62, 152.84, 152.66, 152.24, 151.30, 149.78, 139.54, 136.10, 130.61, 130.04, 129.17, 128.07, 127.68, 126.74, 125.58, 125.11, 124.55, 124.04, 122.07, 121.85, 119.41, 117.35, 109.19, 104.72, 101.68, 97.35, 83.73, 44.27, 26.93, 19.88, 12.79. HRMS (ESI) for [C₆₄H₄₈F₆N₄O₆Pt]²⁺: calcd 638.65574, Found 638.65605. Elemental analysis calcd (%) for C₆₄H₄₆F₆N₄O₆Pt•CH₂Cl₂: C, 57.36; H, 3.55; N, 5.21; found: C, 57.21; H, 3.56; N, 5.13.

Synthesis of complex 4 [Pt($t\text{Bu}_2$ -bpy)(L2)₂]. The synthetic procedure was similar to that of complex **1** except that **L2** was used instead of **L1**. Yield: 237 mg, 20.5%). ¹H NMR (400 MHz, DMSO) δ 9.20 (d, J = 6.0 Hz, 2H), 8.60 (d, J = 1.6 Hz, 2H), 8.05-8.00 (m, 2H), 7.86-7.82 (m, 2H), 7.79-7.70 (m, 4H), 7.40-7.36 (m, 2H), 7.36-7.32 (m, 2H), 7.29 (dd, J = 8.5, 1.3 Hz, 2H), 6.58-6.43 (m, 8H), 3.41-3.36 (m, 8H), 1.40 (s, 18H), 1.11 (t, J = 7.0 Hz, 12H). ¹³C NMR (125 MHz, DMSO) δ 169.17, 164.62, 156.10, 152.65, 150.13, 149.82, 149.37, 136.25, 134.04, 130.73, 130.01, 129.19, 126.67, 125.22, 124.62, 123.83, 121.69, 119.53, 117.45, 109.19, 104.54, 99.71, 97.40, 90.63, 83.59, 44.28, 36.39, 31.76, 30.28, 12.80. HRMS (ESI) for [C₇₀H₆₆N₄O₆Pt]²⁺: calcd 626.73096, Found 626.73141. Elemental analysis calcd (%) for C₇₀H₆₄N₄O₆Pt•CH₃CN: C, 66.86; H, 5.22; N, 5.41; found: C, 66.72; H, 5.56; N, 5.35.

Synthesis of complex 5 [Pt(bpy)(L2)₂]. The synthetic procedure was similar to that of complex **2** except that **L2** was used instead of **L1**. Yield: 184 mg, 16.2%. ¹H NMR (400 MHz, DMSO) δ 9.34 (d, J = 4.7 Hz, 2H), 8.62 (d, J = 8.3 Hz, 2H), 8.37 (td, J = 7.9, 1.5 Hz, 2H), 8.03 (dd, J = 9.1, 8.2 Hz, 2H), 7.86-7.82 (m, 2H), 7.76 (t, J = 7.2 Hz, 4H), 7.39 (dd, J = 8.6, 1.9 Hz, 2H), 7.36 (dd,

J = 7.6, 2.5 Hz, 2H), 7.31 (dd, *J* = 8.6, 1.6 Hz, 2H), 6.56-6.45 (m, 8H), 3.42-3.35 (m, 8H), 1.11 (t, *J* = 7.0 Hz, 12H). ^{13}C NMR (125 MHz, DMSO) δ 169.15, 156.30, 152.65, 150.49, 149.82, 149.44, 140.58, 136.23, 134.08, 130.73, 130.12, 129.19, 128.62, 126.68, 125.22, 124.61, 124.42, 123.71, 119.58, 117.47, 109.19, 104.56, 99.87, 97.41, 89.79, 83.56, 44.28, 12.80. HRMS (ESI) for $[\text{C}_{62}\text{H}_{50}\text{N}_4\text{O}_6\text{Pt}]^{2+}$: calcd 570.66836, Found 570.66862. Elemental analysis calcd (%) for $\text{C}_{62}\text{H}_{48}\text{N}_4\text{O}_6\text{Pt} \bullet \text{CH}_3\text{CN}$: C, 65.08; H, 4.35; N, 5.93; found: C, 65.14; H, 4.19; N, 5.87.

Synthesis of complex 6 [Pt{($\text{CF}_3)_2$ -bpy}(L2)₂]. The synthetic procedure was similar to that of complex **3** except that **L2** was used instead of **L1**. Yield: 255 mg, 20.3%. ^1H NMR (400 MHz, DMSO) δ 9.62 (d, *J* = 5.8 Hz, 2H), 9.32 (s, 2H), 8.22 (d, *J* = 5.6 Hz, 2H), 8.05 (d, *J* = 7.7 Hz, 1H), 8.02 (d, *J* = 7.7 Hz, 1H) 7.84 (dd, *J* = 13.8, 6.8 Hz, 2H), 7.76 (t, *J* = 7.5 Hz, 2H), 7.45-7.41 (m, 2H), 7.36-7.31 (m, 4H), 6.54 (d, *J* = 1.7 Hz, 2H), 6.53-6.47 (m, 6H), 3.42-3.34 (m, 8H), 1.11 (t, *J* = 7.0 Hz, 12H). ^{13}C NMR (125 MHz, DMSO) δ 169.14, 157.43, 152.60, 152.18, 149.82, 149.63, 138.78, 136.24, 134.28, 130.72, 130.13, 129.16, 126.65, 125.31, 124.60, 123.31, 121.78, 119.58, 117.51, 109.23, 104.58, 97.40, 88.47, 83.51, 44.28, 27.02, 23.15, 12.80. HRMS (ESI) for $[\text{C}_{64}\text{H}_{48}\text{F}_6\text{N}_4\text{O}_6\text{Pt}]^{2+}$: calcd 638.65574, Found 638.65636. Elemental analysis calcd (%) for $\text{C}_{64}\text{H}_{46}\text{F}_6\text{N}_4\text{O}_6\text{Pt} \bullet 2\text{CH}_3\text{CN}$: C, 60.13; H, 3.86; N, 6.19; found: C, 60.19; H, 3.93; N, 6.25.

X-ray Crystallography

Single crystals of complex **4–6** suitable for X-ray diffraction studies were grown by slow vaporized from acetonitrile solution of complex **4–6**. Single-crystal X-ray diffraction analysis of **4–6** was performed on a Bruker APEX-II CCD diffractometer with graphite-monochromated Cu-K α radiation (λ = 1.54178 Å) at 100 K. All absorption corrections were performed using multi-scan. The structure was solved by direct methods and refined by full-matrix least-squares on F² with the SHELXTL-97 program package.^{6,7} CCDC: 2265665–2265667 contains the supplementary crystallographic data for this paper. These data can be obtained free of charge from The Cambridge Crystallographic Data Centre via www.ccdc.cam.ac.uk/data_request/cif.

Computational Details

All geometries and energies presented in this study were computed using the B3PW91^{8,9} density functional theory method with DFT-D3^{10,11} dispersion correction as implemented in the ORCA4 program.¹² Geometry optimizations were performed using basis set def2svp, and the stationary structures are obtained by verifying that all of the harmonic frequencies are real. The graphics were generated using Multifw¹³ and VMD¹⁴ programs, respectively.

Table S1. Crystal and structure determination data of **4-6**.

	4	5	6
Empirical formula	C ₁₄₀ H ₁₁₇ N ₈ O ₁₂ Pt ₂	C ₆₃ H ₅₀ Cl ₂ N ₄ O ₆ Pt	C ₁₃₀ H ₉₅ F ₁₂ N ₉ O ₁₂ Pt ₂
Formula weight	2493.59	1225.06	2593.32
Temperature, K	100.01	100.0	99.99
Wavelength, Å	1.54178	1.54178	1.54178
Crystal system	Triclinic	Triclinic	Triclinic
Space group	<i>P</i> ī	<i>P</i> ī	<i>P</i> ī
<i>a</i> , Å	8.3256(3)	9.0038(2)	10.8438(5)
<i>b</i> , Å	18.5591(8)	14.4319(3)	15.9016(8)
<i>c</i> , Å	21.9298(8)	21.8553(5)	17.1632(8)
α , deg	99.743(2)	85.4570(10)	97.148(2)
β , deg	92.001(2)	86.5640(10)	101.302(2)
γ , deg	94.383(2)	81.1880(10)	103.266(3)
Volume, Å ³	3325.9(2)	2794.29(11)	2779.8(2)
<i>Z</i>	1	2	1
Density (calculated), g cm ⁻³	1.245	1.456	1.549
Crystal size, mm×mm×mm	0.21×0.19×0.17	0.25×0.13×0.11	0.20×0.14×0.1
Index ranges	$-9 \leq h \leq 9$ $-21 \leq k \leq 20$ $-25 \leq l \leq 25$	$-10 \leq h \leq 10$ $-16 \leq k \leq 16$ $-25 \leq l \leq 25$	$-12 \leq h \leq 12$ $-18 \leq k \leq 15$ $-20 \leq l \leq 20$
Reflections collected/unique	47167 / 11259 [R(int) = 0.0396]	50825 / 9491 [R(int) = 0.0396]	28266 / 9381 [R(int) = 0.0497]
Completeness, %	98.7 (to theta = 67.679°)	99.1 (to theta = 67.679°)	98.5 (to theta = 67.679°)
Data / restraints / parameters	11259 / 241 / 829	9491 / 36 / 689	9381 / 294 / 951
Goodness-of-fit on F^2	1.070	1.137	1.133
Final <i>R</i> indices ^a	$R_1 = 0.0575$	$R_1 = 0.0450$	$R_1 = 0.0584$
[$I > 2\sigma(I)$]	w <i>R</i> ₂ = 0.2933	w <i>R</i> ₂ = 0.1223	w <i>R</i> ₂ = 0.1539
Largest diff. peak and hole, eÅ ⁻³	3.123 and -1.239	2.003 and -1.656	3.717 and -1.038

^a $R_{\text{int}} = \sum |F_o^2 - F_c^2| / \sum [F_o^2]$, $R_1 = \sum ||F_o|| - ||F_c|| / \sum ||F_o||$ and $wR_2 = \{\sum [w(F_o^2 - F_c^2)^2] / \sum [w(F_o^2)^2]\}^{1/2}$.

Table S2. Selected bond lengths (\AA) and angles (deg) for **4-6** with estimated standard deviations (esds) given in parentheses

4			
Bond Lengths (\AA)			
Pt(1)-N(1)	2.053(5)	N(3)-C(36)	1.529(13)
Pt(1)-N(2)	2.046(5)	O(5)-C(70)	1.40(2)
Pt(1)-C(19)	1.949(7)	O(4)-C(50)	1.404(15)
Pt(1)-C(45)	1.942(7)	O(4)-C(55)	1.34(2)
O(1)-C(29)	1.383(8)	C(29)-C(30)	1.375(9)
O(1)-C(24)	1.374(7)	C(29)-C(28)	1.374(9)
N(1)-C(1)	1.337(8)	O(2)-C(27)	1.521(10)
N(2)-C(6)	1.356(7)	O(2)-C(44)	1.390(13)
N(2)-C(10)	1.343(8)	C(50)-O(4A)	1.418(18)
N(3)-C(31)	1.373(8)	C(53)-O(5)	1.598(18)
N(3)-C(34)	1.455(9)	C(62)-N(4)	1.48(3)
N(4A)-C(63)	1.85(3)	C(57)-N(4)	1.36(2)
O(6)-C(70)	1.41(2)	N(4)-C(60)	1.63(2)
Bond Angles (deg)			
N(2)-Pt(1)-N(1)	79.23(19)	C(6)-N(2)-Pt(1)	115.8(4)
C(19)-Pt(1)-N(1)	175.5(2)	C(10)-N(2)-Pt(1)	126.2(4)
C(19)-Pt(1)-N(2)	97.2(2)	C(10)-N(2)-C(6)	117.6(5)
C(45)-Pt(1)-N(1)	96.2(2)	N(2)-C(6)-C(5)	114.5(5)
C(45)-Pt(1)-N(2)	174.0(2)	N(2)-C(6)-C(7)	121.8(5)
C(45)-Pt(1)-C(19)	87.6(3)	C(31)-N(3)-C(34)	121.1(6)
C(24)-O(1)-C(29)	118.4(5)	C(31)-N(3)-C(36)	121.0(6)
C(5)-N(1)-Pt(1)	115.4(4)	C(34)-N(3)-C(36)	117.2(6)
C(1)-N(1)-Pt(1)	126.0(4)	N(1)-C(5)-C(6)	114.4(5)
C(1)-N(1)-C(5)	118.1(5)	N(1)-C(5)-C(4)	120.9(5)
N(1)-C(1)-C(2)	122.9(6)	N(2)-C(10)-C(9)	123.3(6)
C(55)-O(4)-C(50)	116.2(13)	C(46)-C(45)-Pt(1)	177.5(7)
C(30)-C(29)-O(1)	114.5(6)	C(25)-C(27)-O(2)	107.9(6)
C(28)-C(29)-O(1)	123.5(6)	C(28)-C(27)-O(2)	108.4(6)

C(44)-O(2)-C(27)	103.3(8)	C(28)-C(27)-C(25)	112.4(6)
N(3)-C(31)-C(30)	120.9(6)	C(38)-C(27)-O(2)	103.7(6)
N(3)-C(31)-C(32)	121.7(6)	C(49)-C(50)-O(4)	114.7(9)
O(1)-C(24)-C(23)	115.9(6)	C(49)-C(50)-O(4A)	114.1(10)
O(1)-C(24)-C(25)	123.0(6)	C(51)-C(50)-O(4)	122.1(9)
C(20)-C(19)-Pt(1)	177.6(6)	C(51)-C(50)-O(4A)	121.5(10)
O(3)-C(44)-O(2)	114.3(11)	C(37)-C(36)-N(3)	107.2(10)
O(3)-C(44)-C(43)	131.0(12)	N(4)-C(57)-C(58)	120.6(16)
C(43)-C(44)-O(2)	114.6(10)	C(61)-C(60)-N(4)	96(2)
C(51)-C(53)-O(5)	104.2(11)	O(5)-C(70)-O(6)	105.0(17)
C(54)-C(53)-O(5)	95.4(11)	C(69)-C(70)-O(5)	117.0(18)
O(5)-C(53)-C(54A)	119.5(12)	C(69)-C(70)-O(6)	138(2)
C(64)-C(53)-O(5)	101.9(10)	C(62A)-C(63)-N(4A)	96(2)
O(4)-C(55)-C(54)	123.6(15)	N(4)-C(62)-C(63)	101.5(16)
O(4)-C(55)-C(56)	115.0(16)	N(4)-C(57)-C(56)	121.9(17)

5

Bond Lengths (Å)			
Pt(1)-N(1)	2.061(4)	O(5)-C(45)	1.541(9)
Pt(1)-N(2)	2.055(4)	O(5)-C(62)	1.312(11)
Pt(1)-C(11)	1.949(5)	O(3)-C(36)	1.227(9)
Pt(1)-C(37)	1.956(6)	N(3)-C(23)	1.376(7)
O(1)-C(16)	1.370(6)	N(3)-C(26)	1.472(9)
O(1)-C(21)	1.384(7)	N(3)-C(28)	1.450(9)
O(4)-C(42)	1.379(7)	O(6)-C(62)	1.219(11)
O(4)-C(47)	1.390(7)	O(5)-C(45)	1.541(9)
N(1)-C(1)	1.335(7)	O(2)-C(36)	1.344(8)
N(1)-C(5)	1.358(7)	N(4)-C(49)	1.375(8)
N(2)-C(6)	1.362(7)	N(4)-C(54)	1.451(8)
N(2)-C(10)	1.347(8)	N(4)-C(52)	1.459(9)
O(2)-C(19)	1.510(7)		
Bond Angles (deg)			
N(2)-Pt(1)-N(1)	79.18(18)	C(54)-N(4)-C(52)	116.0(5)
C(11)-Pt(1)-N(1)	96.2(2)	C(62)-O(5)-C(45)	110.7(7)
C(11)-Pt(1)-N(2)	175.40(19)	O(1)-C(16)-C(17)	123.2(5)

C(11)-Pt(1)-C(37)	89.0(2)	O(1)-C(16)-C(15)	115.9(5)
C(37)-Pt(1)-N(1)	173.63(19)	C(12)-C(11)-Pt(1)	178.6(5)
C(16)-O(1)-C(21)	118.7(5)	N(1)-C(1)-C(2)	121.6(6)
C(42)-O(4)-C(47)	117.8(5)	C(43)-C(42)-O(4)	123.8(5)
C(1)-N(1)-Pt(1)	125.4(4)	C(41)-C(42)-O(4)	115.2(5)
C(1)-N(1)-C(5)	119.5(5)	C(48)-C(47)-O(4)	113.4(5)
C(5)-N(1)-Pt(1)	115.0(4)	C(46)-C(47)-O(4)	123.2(5)
C(6)-N(2)-Pt(1)	115.3(4)	N(1)-C(5)-C(6)	115.4(5)
C(10)-N(2)-Pt(1)	125.3(4)	N(1)-C(5)-C(4)	120.8(6)
C(10)-N(2)-C(6)	119.4(5)	C(38)-C(37)-Pt(1)	175.0(5)
C(36)-O(2)-C(19)	110.0(5)	C(23)-N(3)-C(26)	120.0(5)
C(49)-N(4)-C(54)	123.0(6)	C(23)-N(3)-C(28)	120.2(6)
N(2)-C(6)-C(7)	120.1(6)	C(28)-N(3)-C(26)	118.5(5)
N(4)-C(49)-C(48)	121.4(6)	N(2)-C(6)-C(5)	114.9(5)
N(4)-C(49)-C(50)	121.3(6)		

6

Bond Lengths (Å)

Pt(1)-N(1)	2.051(5)	O(4)-C(49)	1.374(10)
Pt(1)-N(2)	2.074(6)	N(1)-C(1)	1.338(9)
Pt(1)-C(13)	1.966(8)	N(1)-C(5)	1.372(9)
Pt(1)-C(39)	1.941(7)	N(2)-C(6)	1.349(9)
F(4)-C(12)	1.328(11)	N(2)-C(10)	1.339(10)
F(5)-C(12)	1.331(10)	N(3)-C(25)	1.385(11)
F(6)-C(12)	1.332(10)	N(3)-C(28)	1.436(13)
O(1)-C(18)	1.360(9)	N(3)-C(30)	1.480(13)
O(1)-C(23)	1.381(9)	N(4)-C(51)	1.365(11)
O(4)-C(44)	1.379(10)	N(4)-C(56)	1.437(12)
N(4)-C(54)	1.71(3)	N(5)-C(65)	1.10(3)
C(11)-F(1)	1.35(3)	C(11)-F(3)	1.435(16)
C(11)-F(2)	1.273(13)	O(6)-C(64)	1.22(2)

Bond Angles (deg)

N(1)-Pt(1)-N(2)	79.0(2)	C(5)-N(1)-Pt(1)	115.4(4)
C(13)-Pt(1)-N(1)	93.9(2)	C(6)-N(2)-Pt(1)	114.5(5)
C(13)-Pt(1)-N(2)	172.7(2)	C(10)-N(2)-Pt(1)	125.5(5)

C(39)-Pt(1)-N(1)	175.1(3)	C(10)-N(2)-C(6)	119.9(6)
C(39)-Pt(1)-N(2)	96.2(3)	C(25)-N(3)-C(28)	119.4(8)
C(39)-Pt(1)-C(13)	90.9(3)	C(25)-N(3)-C(30)	120.9(8)
C(18)-O(1)-C(23)	118.3(5)	C(28)-N(3)-C(30)	118.2(8)
C(49)-O(4)-C(44)	118.3(7)	C(51)-N(4)-C(56)	122.1(9)
C(1)-N(1)-Pt(1)	125.8(5)	C(51)-N(4)-C(54)	115.5(12)
C(1)-N(1)-C(5)	118.8(6)	C(56)-N(4)-C(54)	117.5(11)
N(1)-C(1)-C(2)	122.5(7)	F(2)-C(11)-F(3)	102.3(10)
N(1)-C(5)-C(4)	120.4(7)	F(3)-C(11)-C(3)	106.1(9)
N(1)-C(5)-C(6)	114.5(6)	F(4)-C(12)-F(5)	106.9(8)
N(2)-C(6)-C(5)	116.2(6)	F(4)-C(12)-F(6)	106.0(7)
N(2)-C(6)-C(7)	120.8(6)	F(4)-C(12)-C(8)	114.3(7)
N(2)-C(10)-C(9)	121.8(7)	F(5)-C(12)-F(6)	106.0(7)
F(1)-C(11)-C(3)	110.1(12)	F(5)-C(12)-C(8)	110.8(7)
F(1)-C(11)-F(3)	128.2(17)	F(6)-C(12)-C(8)	112.3(7)
F(2)-C(11)-C(3)	113.4(9)	C(14)-C(13)-Pt(1)	170.1(6)
F(2)-C(11)-F(1)	95.9(17)	O(1)-C(18)-C(17)	115.0(6)
O(1)-C(18)-C(19)	123.8(6)	O(4)-C(49)-C(48)	123.3(7)
O(1)-C(23)-C(22)	122.6(7)	O(4)-C(49)-C(50)	115.6(8)
O(1)-C(23)-C(24)	114.3(6)	N(4)-C(51)-C(50)	121.7(9)
N(3)-C(25)-C(24)	120.7(8)	N(4)-C(51)-C(52)	121.4(8)
N(3)-C(25)-C(26)	121.3(8)	N(4)-C(56)-C(57)	114.5(10)
C(29)-C(28)-N(3)	112.5(12)	C(38)-O(2)-C(21)	105.0(13)
N(3)-C(30)-C(31)	114.2(11)	C(64)-O(5)-C(47)	112.3(14)
C(40)-C(39)-Pt(1)	175.8(7)	O(2)-C(21)-C(19)	112.4(14)
O(4)-C(44)-C(43)	115.5(7)	O(2)-C(21)-C(22)	116.4(15)
C(45)-C(44)-O(4)	122.5(7)	O(2)-C(21)-C(32)	106.4(13)
O(2)-C(38)-C(37)	116.4(12)	C(55)-C(54)-N(4)	108(2)
O(3)-C(38)-O(2)	113.6(18)	O(5)-C(64)-C(63)	105.9(15)
O(3)-C(38)-C(37)	130.0(19)	O(6)-C(64)-O(5)	123(2)
C(45)-C(47)-C(48)	109.2(9)	O(6)-C(64)-C(63)	131(2)
C(45)-C(47)-O(5)	110.8(10)	N(5)-C(65)-C(66)	175(3)
C(48)-C(47)-O(5)	111.7(9)	C(58)-C(47)-O(5)	102.3(10)

Table S3. Calculated structural data of **1** and **4**.

	1			4		
	Pt-C α	C α -C β	C β -C γ	Pt-C α	C α -C β	C β -C γ
Bond distance of Ring-closed form (\AA)	1.94	1.23	1.43	1.94	1.23	1.43
Bond distance of Ring-opened form (\AA)	1.94	1.23	1.41	1.94	1.23	1.43
Δ distance = Closed form – opened form (\AA)	0.00	0.00	+0.02	0.00	0.00	0.00

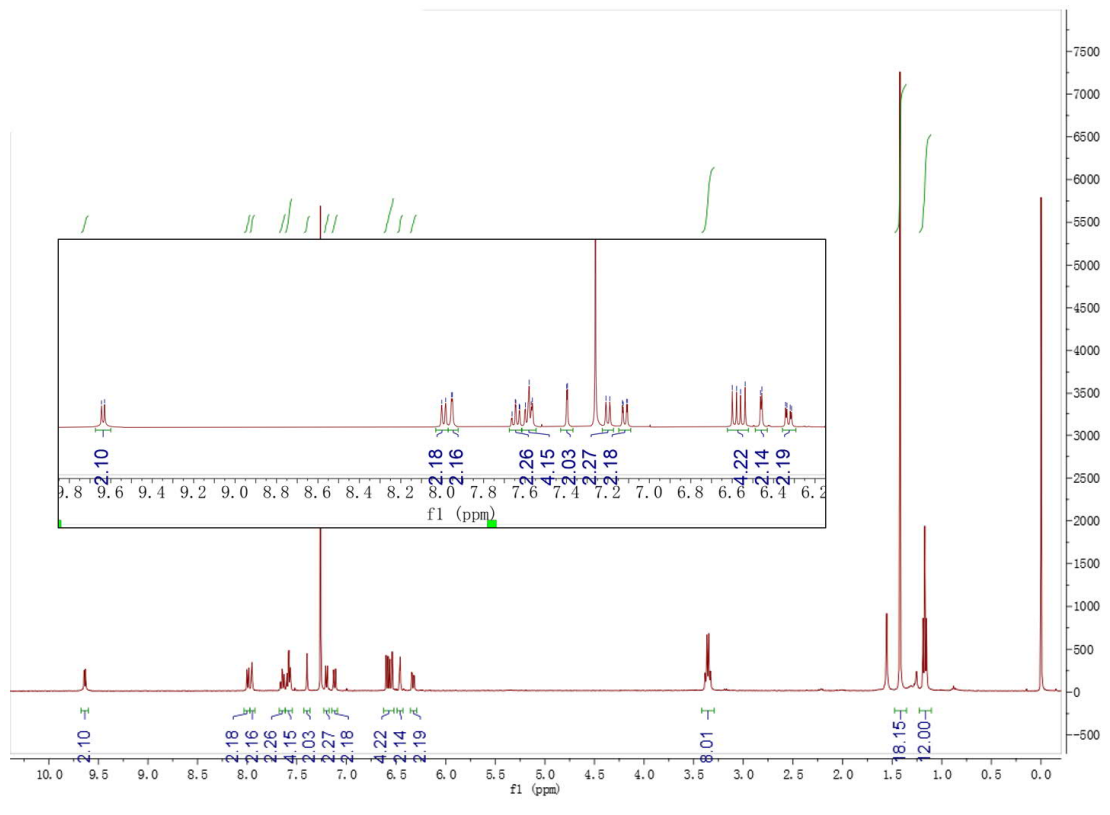


Figure S1. ^1H NMR spectrum of **1** in DMSO.

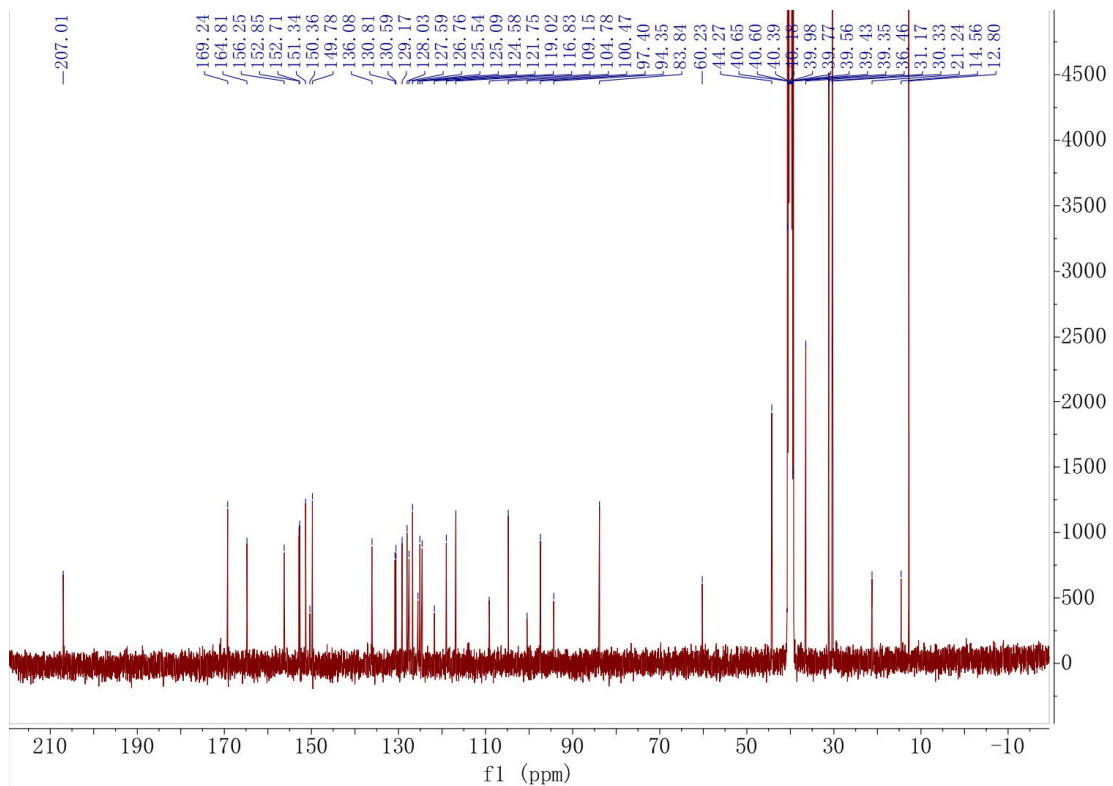


Figure S2. ^{13}C NMR spectrum of 1 in DMSO.

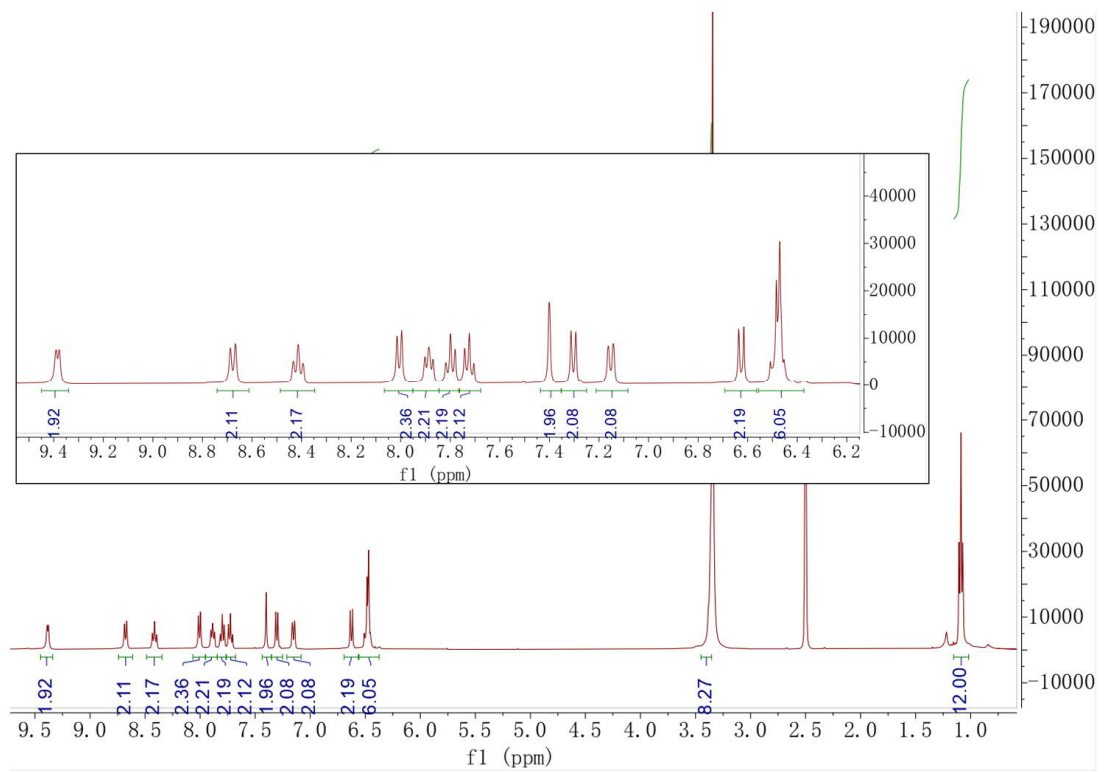


Figure S3. ¹H NMR spectrum of **2** in DMSO.

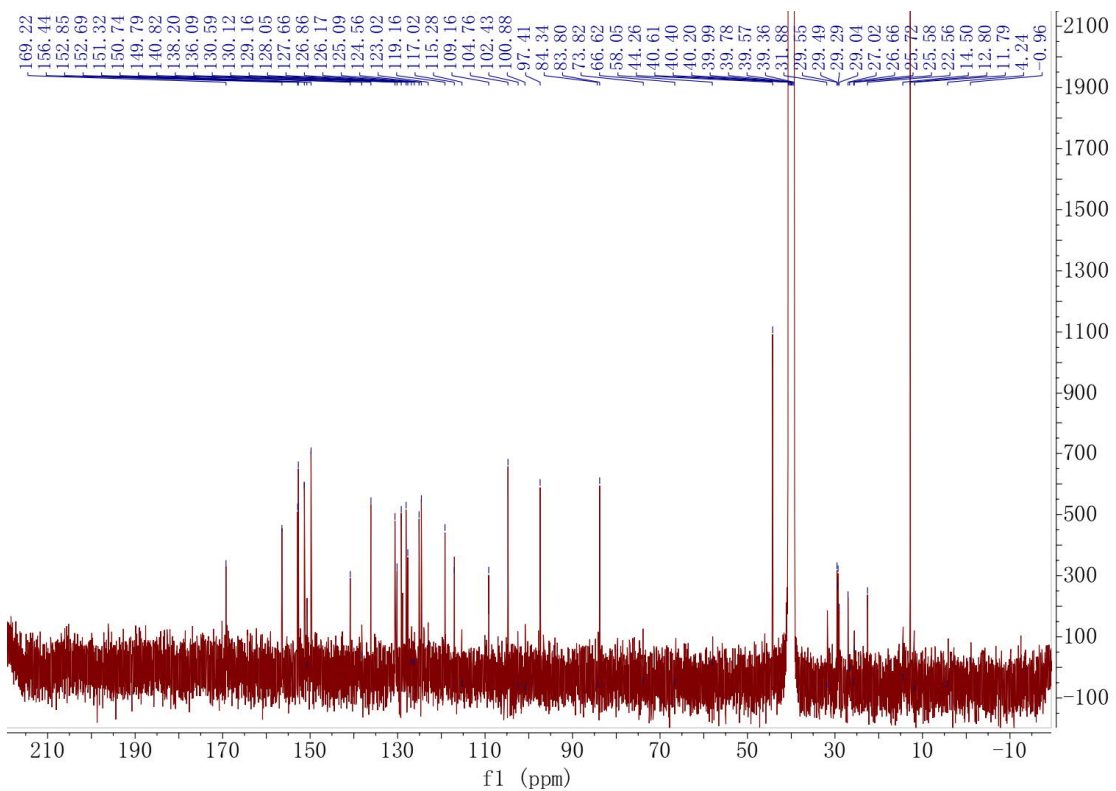


Figure S4. ^{13}C NMR spectrum of **2** in DMSO.

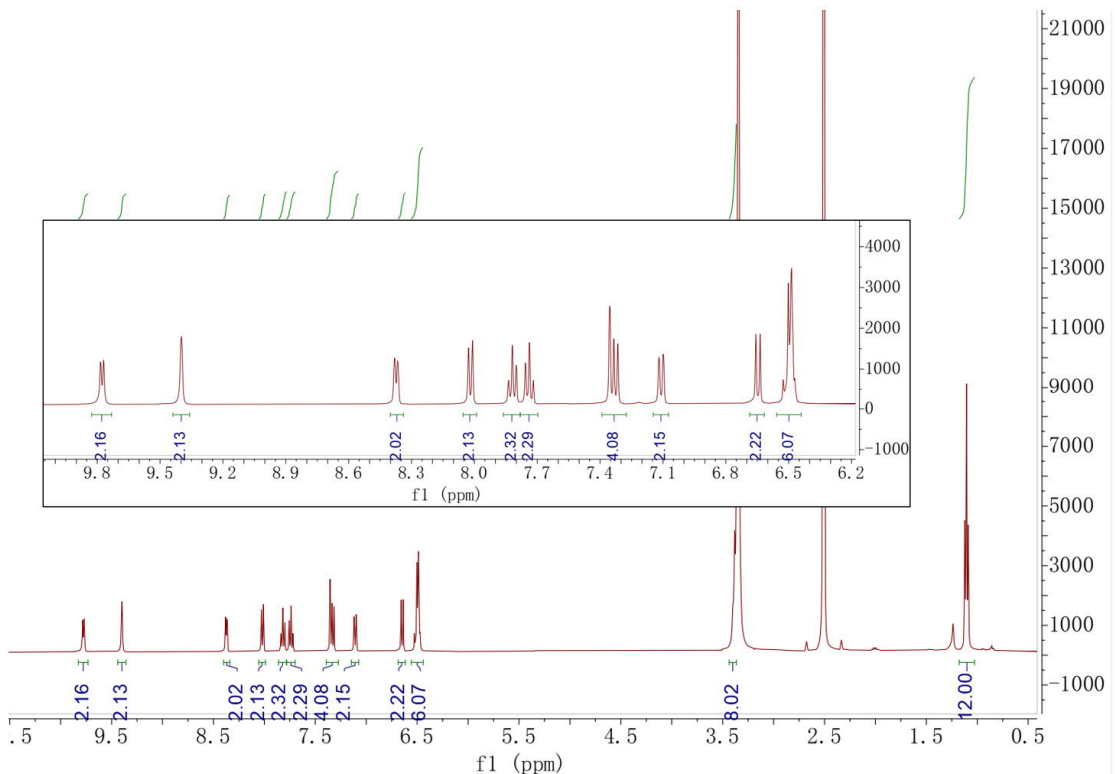


Figure S5. ¹H NMR spectrum of **3** in DMSO.

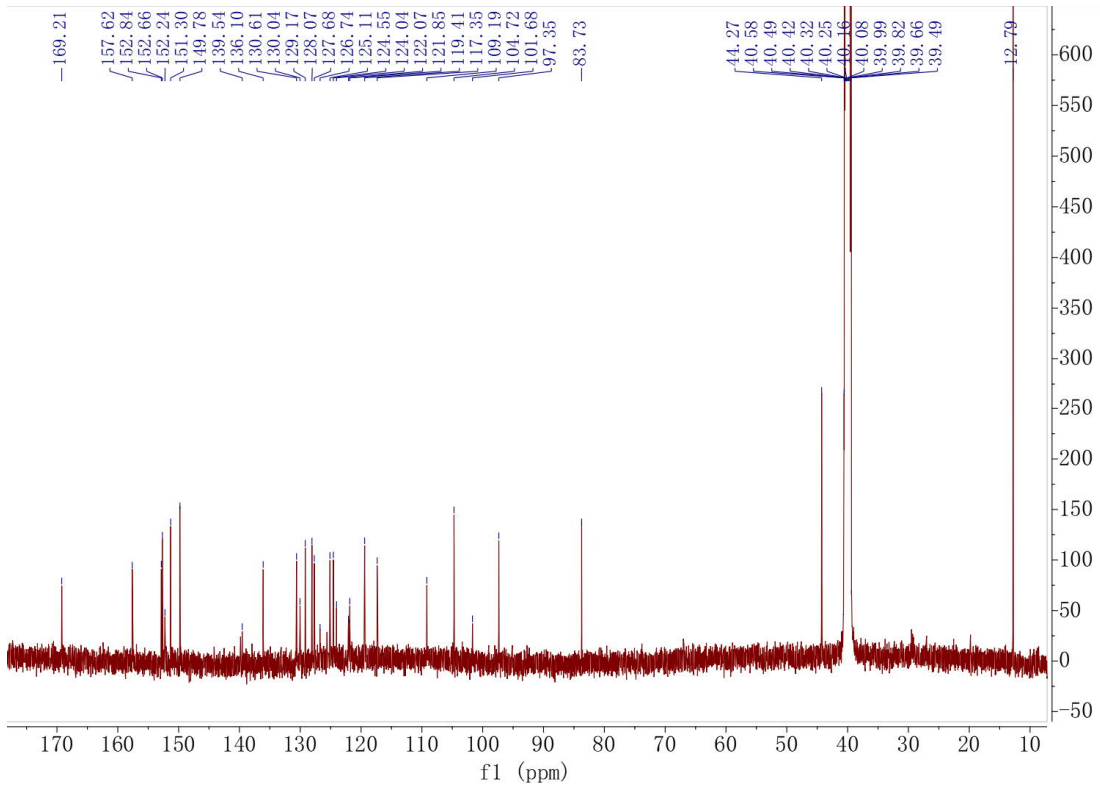


Figure S6. ¹³C NMR spectrum of **3** in DMSO.

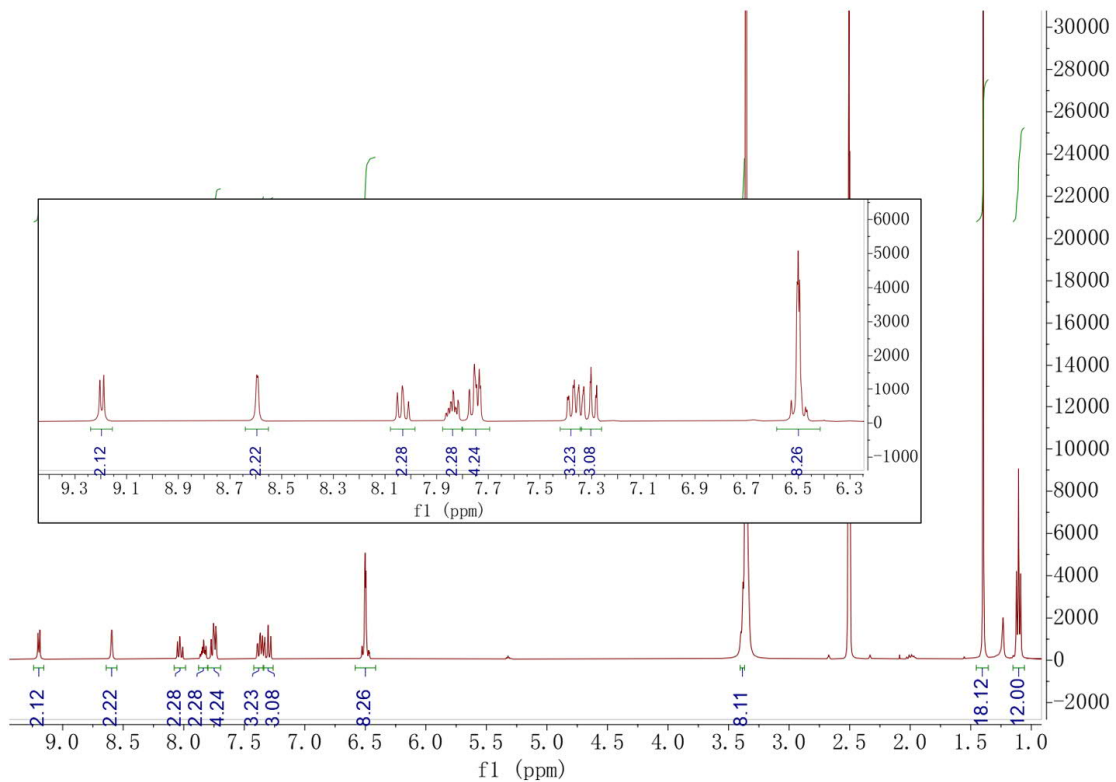


Figure S7. ¹H NMR spectrum of **4** in DMSO.

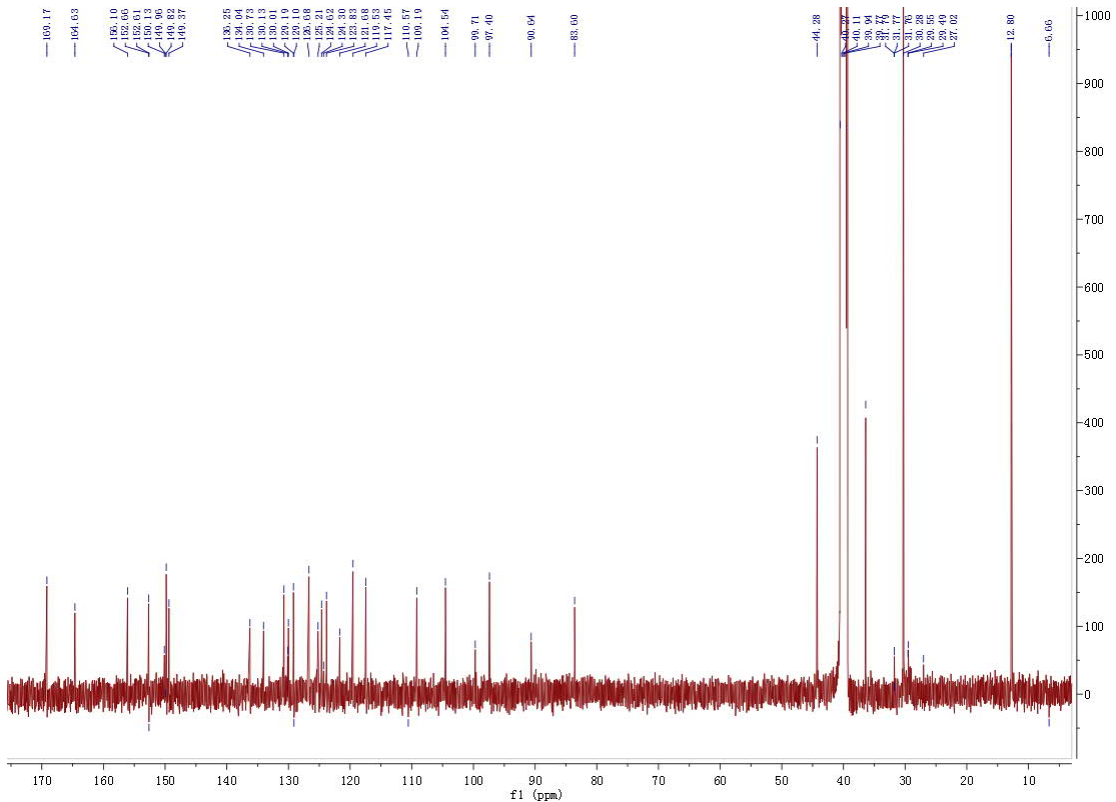


Figure S8. ¹³C NMR spectrum of **4** in DMSO.

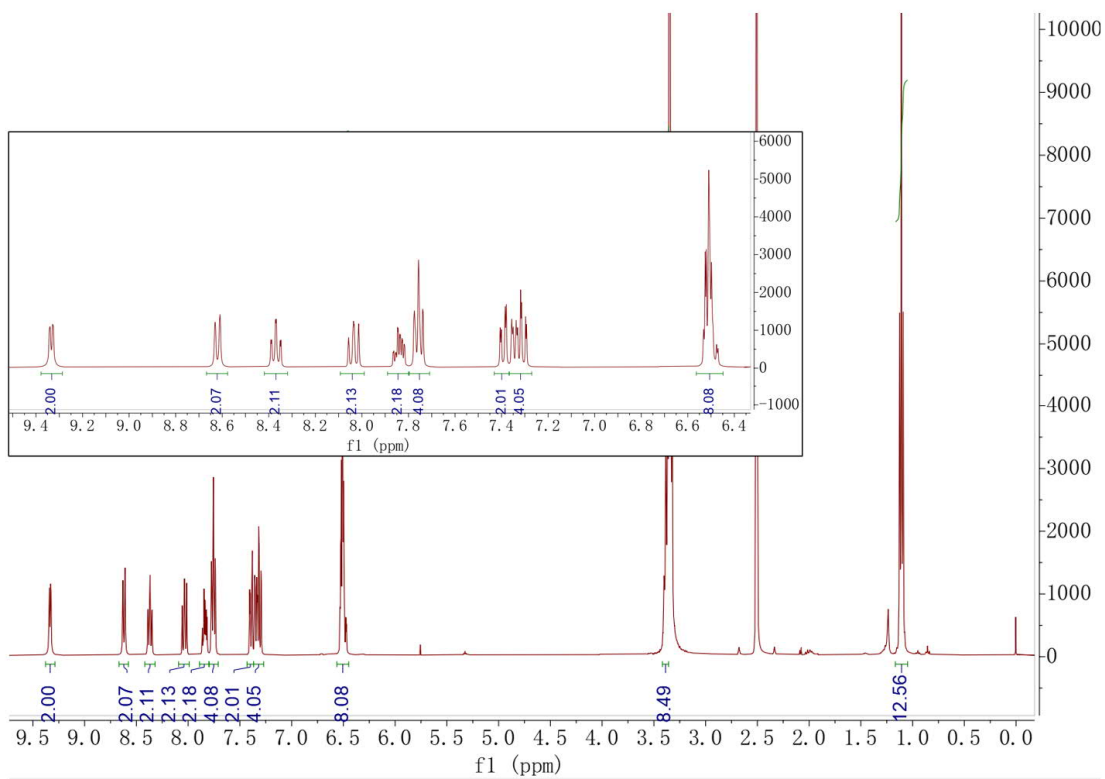


Figure S9. ¹H NMR spectrum of **5** in DMSO.

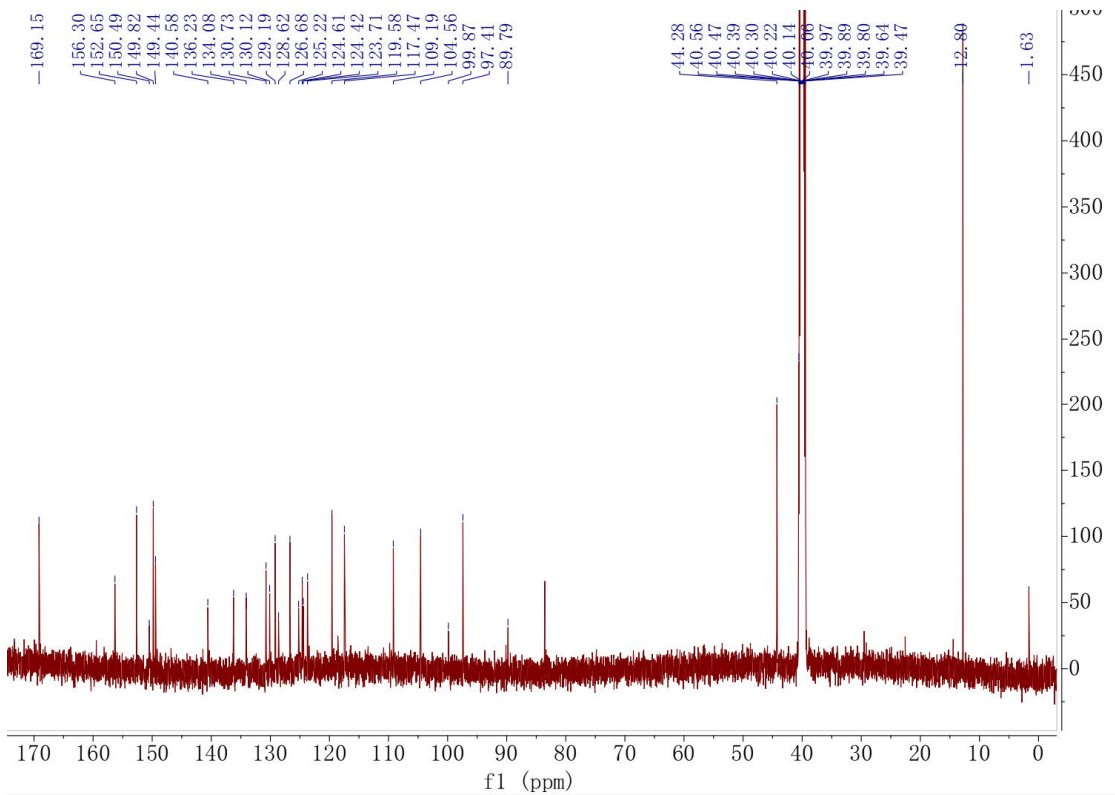


Figure S10. ^{13}C NMR spectrum of **5** in DMSO.

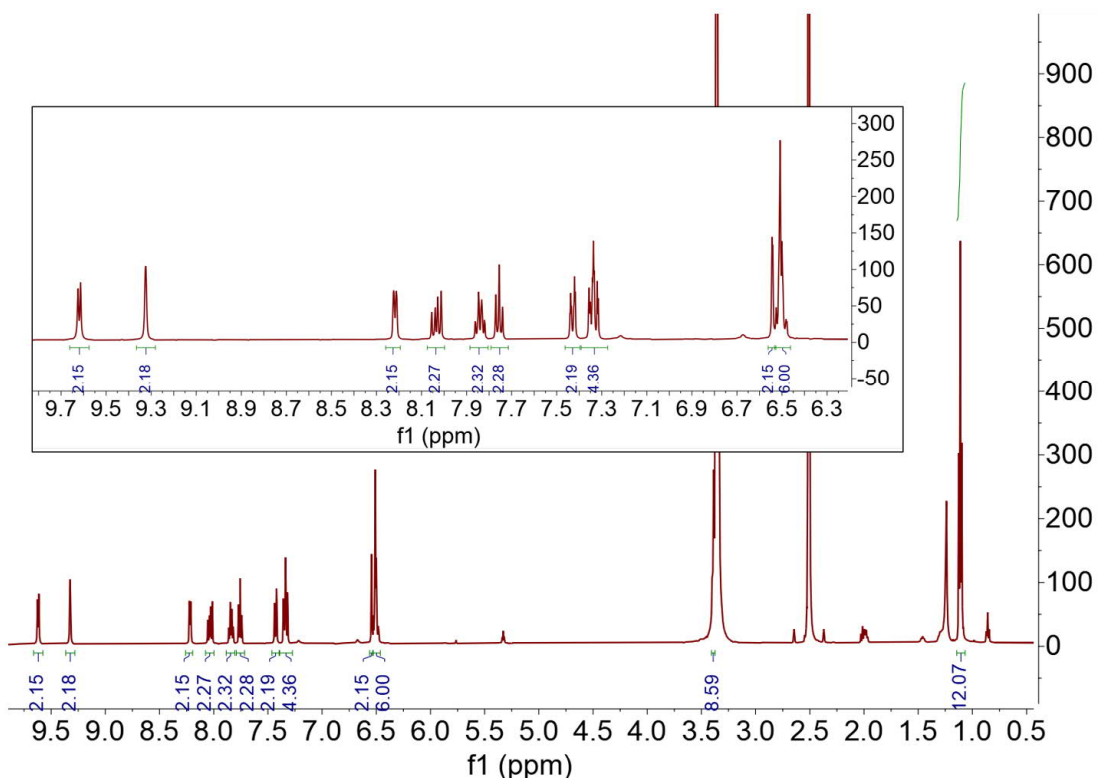


Figure S11. ¹H NMR spectrum of **6** in DMSO.

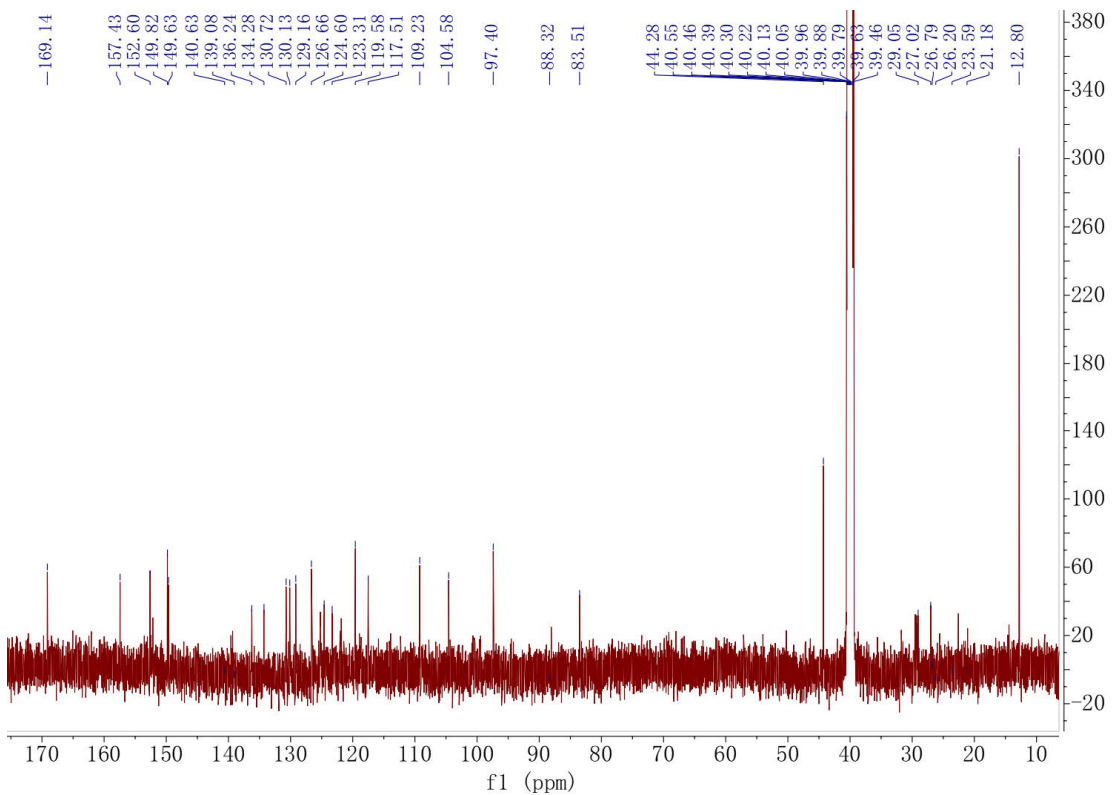
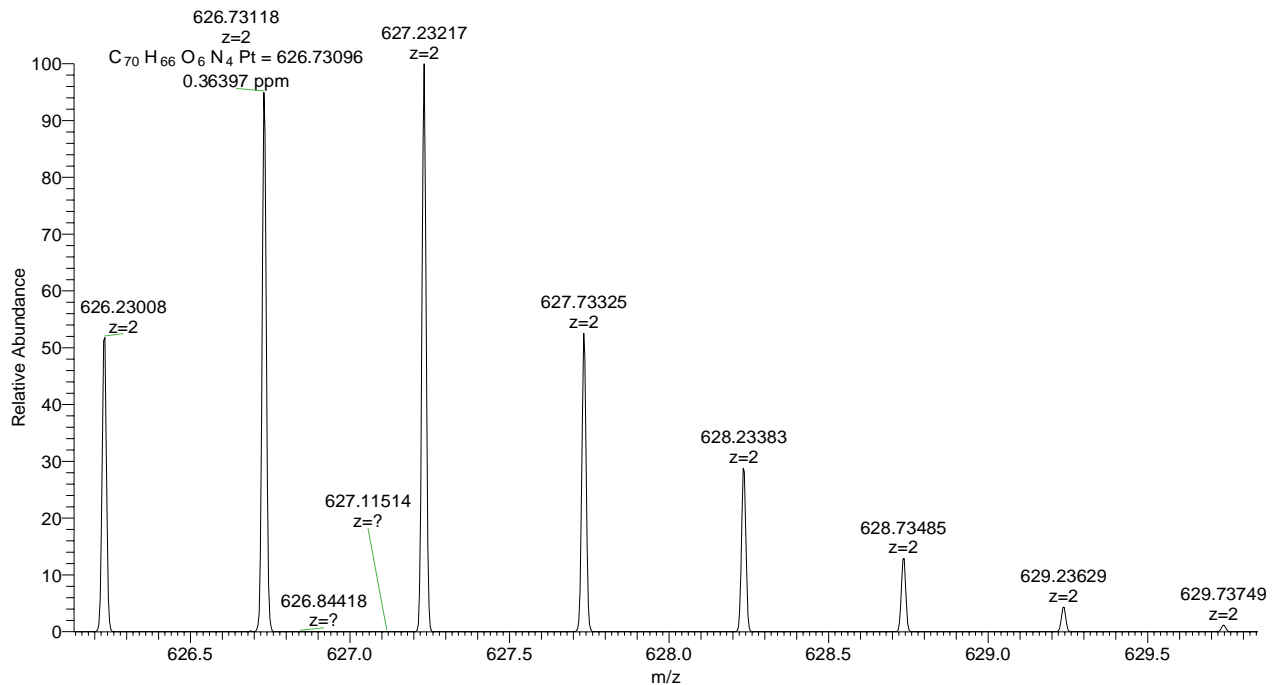


Figure S12. ^{13}C NMR spectrum of **6** in DMSO.

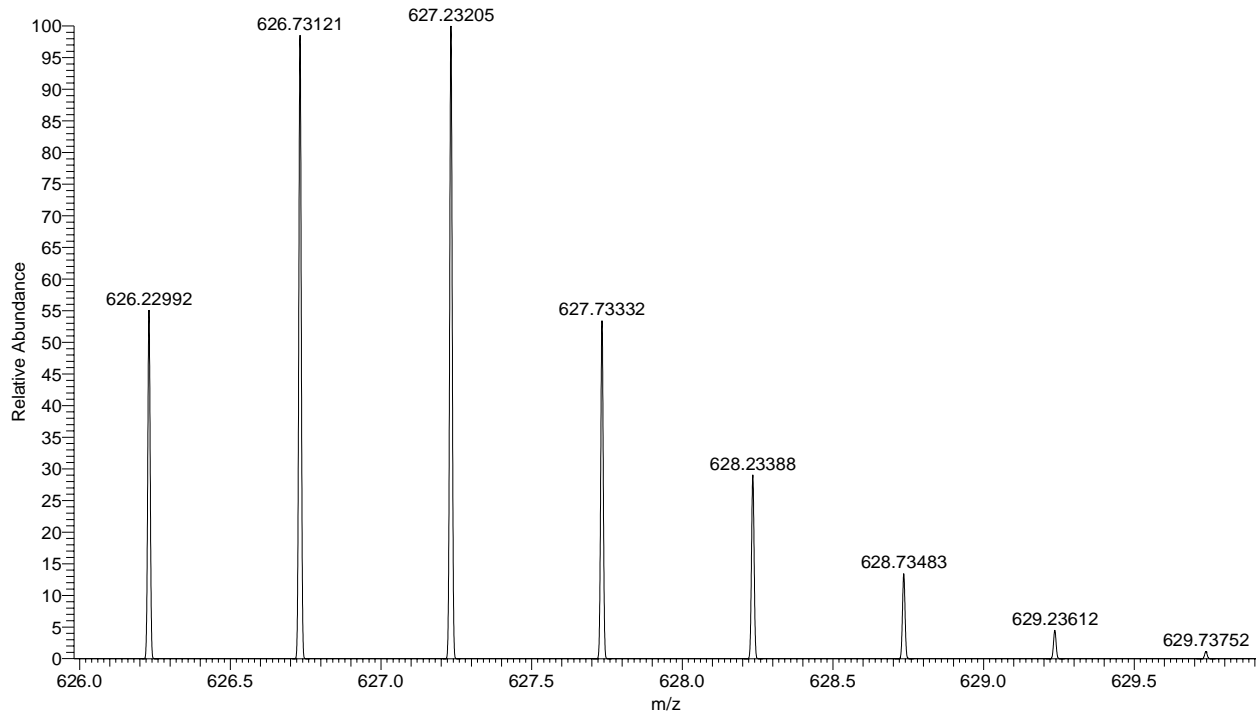
(a) $[1+2H]^{2+}$

zhaoshunan-20220929-1 #11-25 RT: 0.05-0.11 AV: 15 NL: 7.11E8
T: FTMS + p ESI Full ms [100.0000-1500.0000]



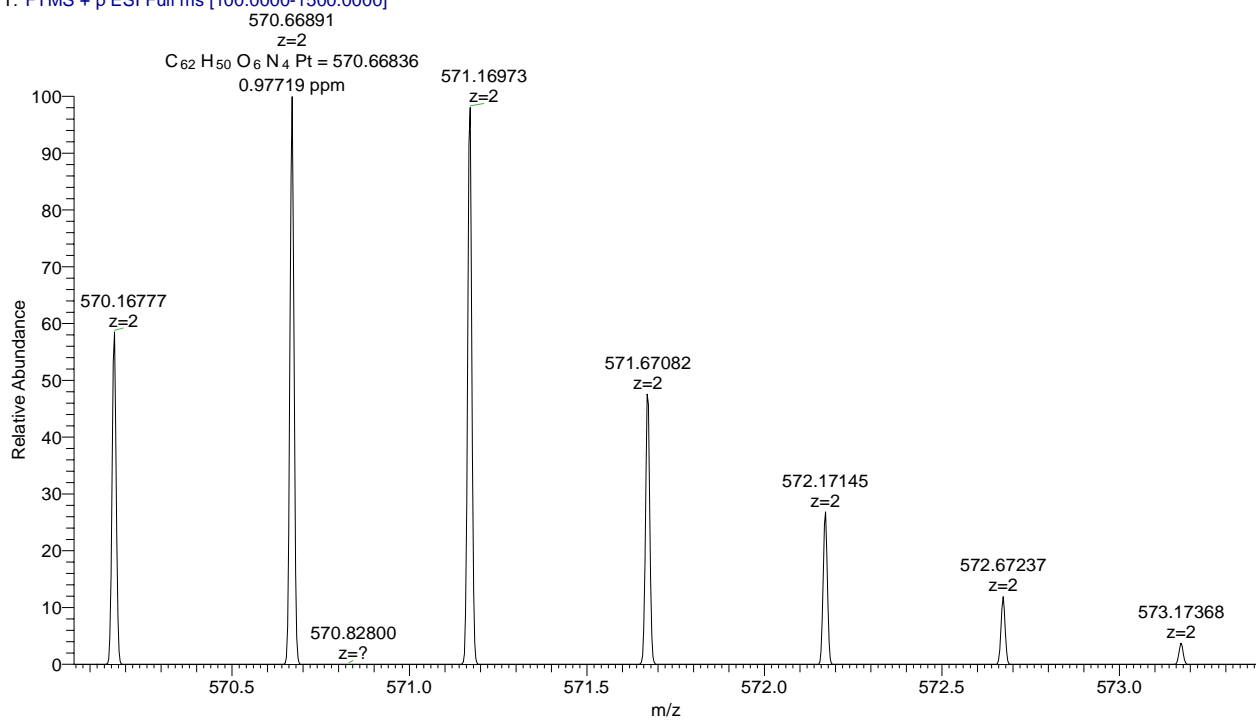
Theoretical isotope pattern of $[C_{70}H_{66}N_4O_6Pt]^{2+}$

C70H64N4O6Pt +H: C70 H66 N4 O6 Pt1 p(gss, s/p:40) Ch...



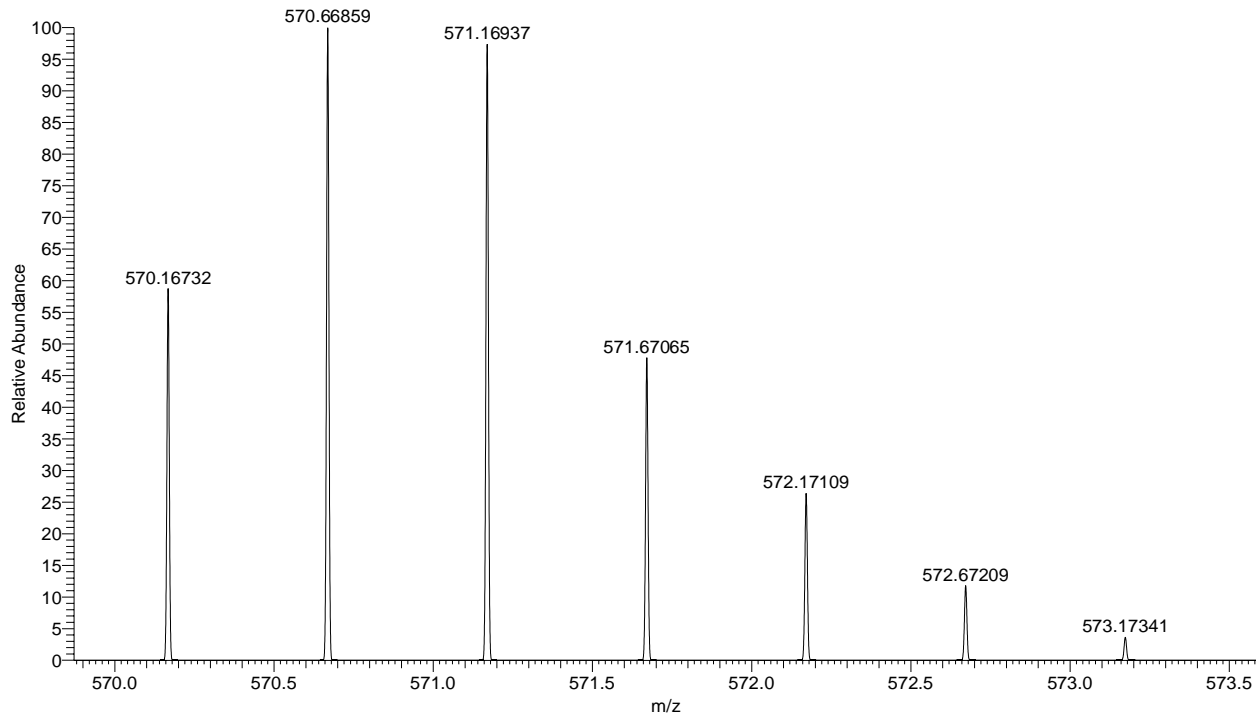
(b) [2+2H]²⁺

zhaoshunyan-20220929-2 #8-29 RT: 0.03-0.13 AV: 22 NL: 3.55E8
 T: FTMS + p ESI Full ms [100.0000-1500.0000]



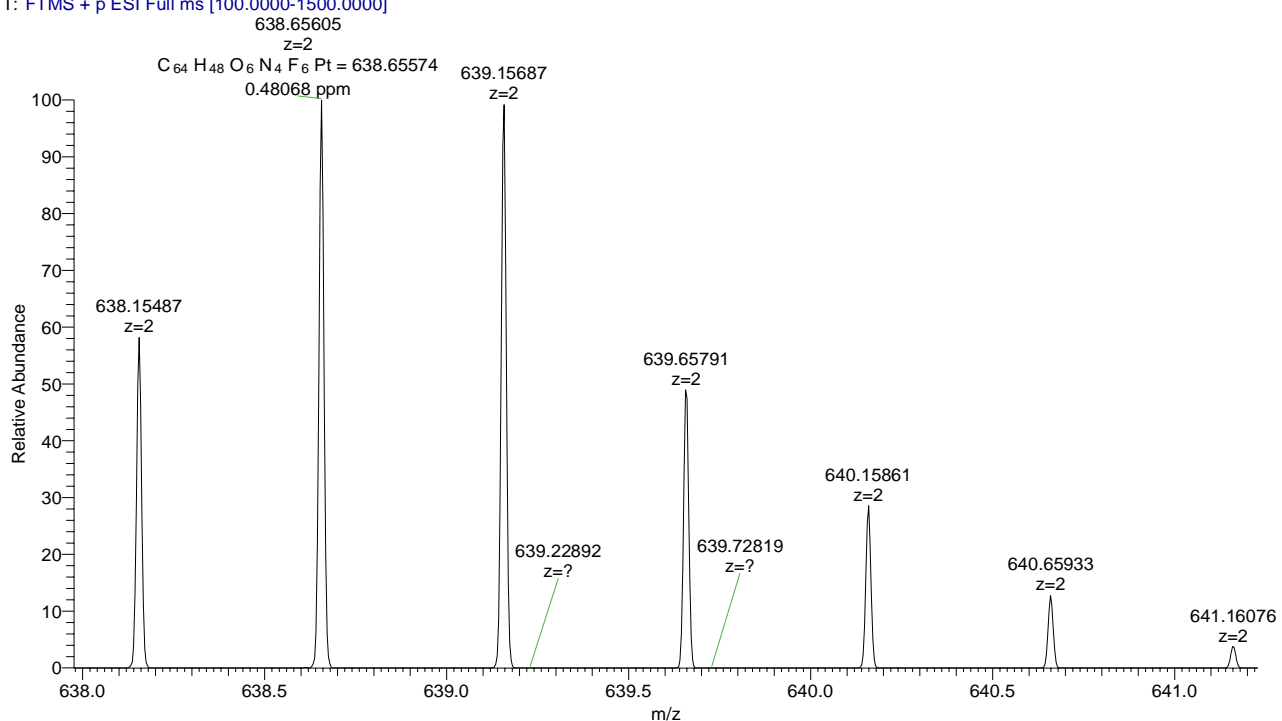
Theoretical isotope pattern of [C₆₂H₅₀N₄O₆Pt]²⁺

C62H48N4O6Pt +H: C62 H50 N4 O6 Pt1 p(gss, s/p:40) Ch...



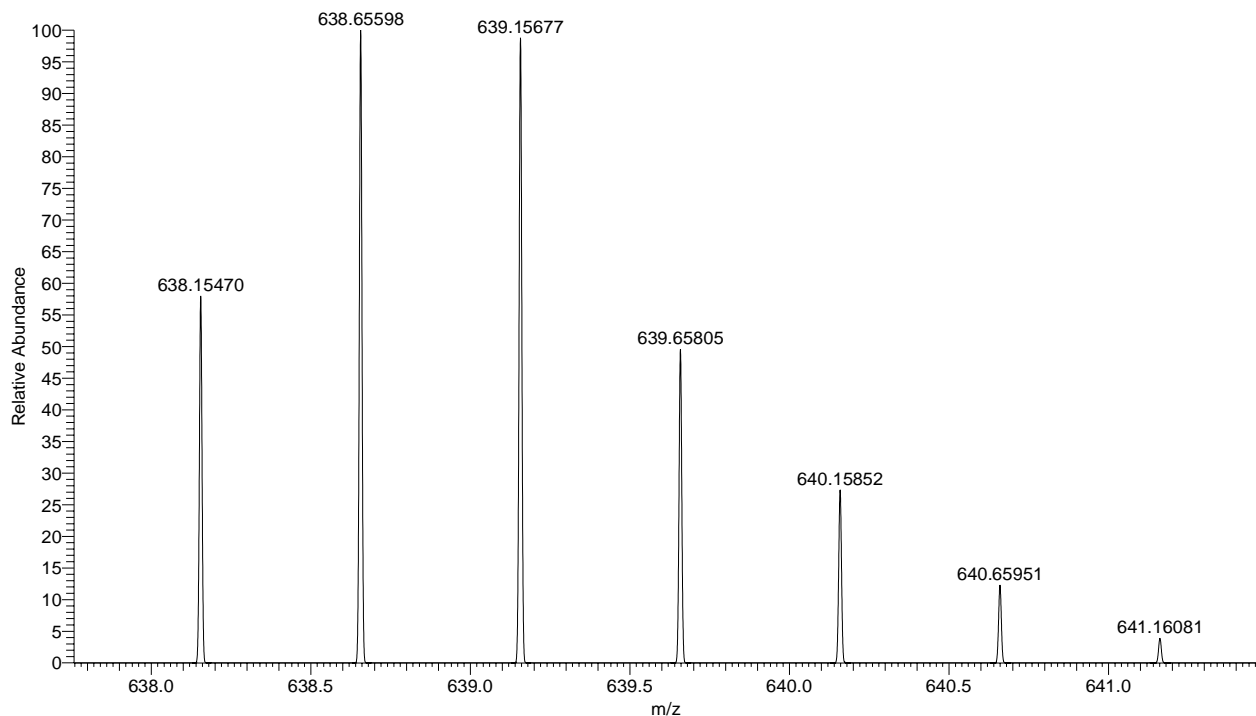
(c) [3+2H]²⁺

zhaoshunan-20220929-3 #10-32 RT: 0.04-0.14 AV: 23 NL: 3.50E8
 T: FTMS + p ESI Full ms [100.0000-1500.0000]



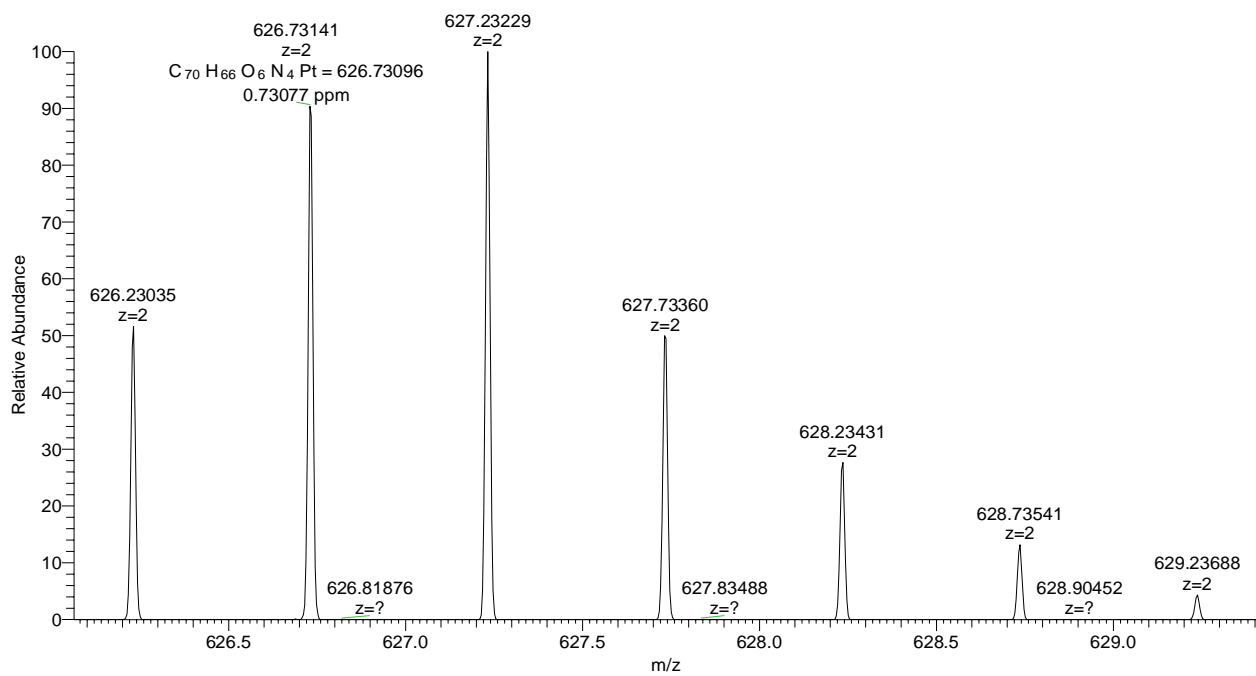
Theoretical isotope pattern of [C₆₄H₄₈F₆N₄O₆Pt]²⁺

C64H46F6N4O6Pt +H: C64 H48 F6 N4 O6 Pt1 p(gss, s/p:4...



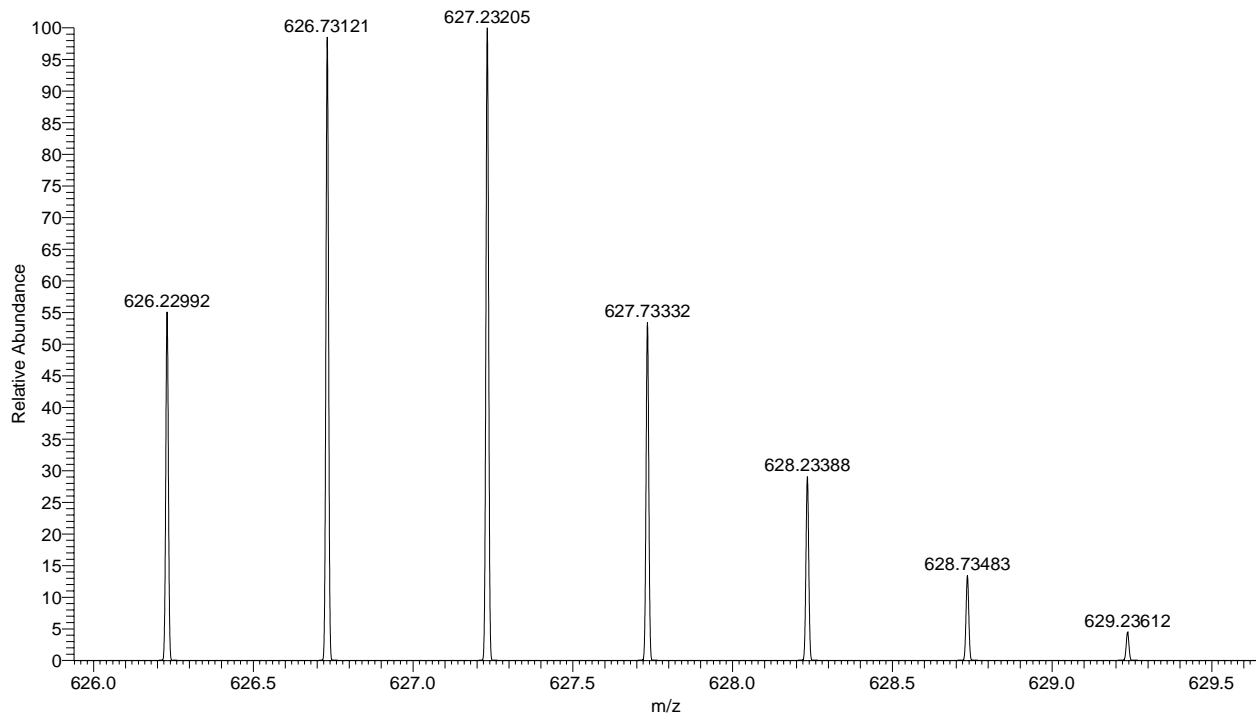
(d) $[4+2H]^{2+}$

zhaoshunan-20220929-4 #9-27 RT: 0.04-0.12 AV: 19 NL: 2.67E8
T: FTMS + p ESI Full ms [100.0000-1500.0000]



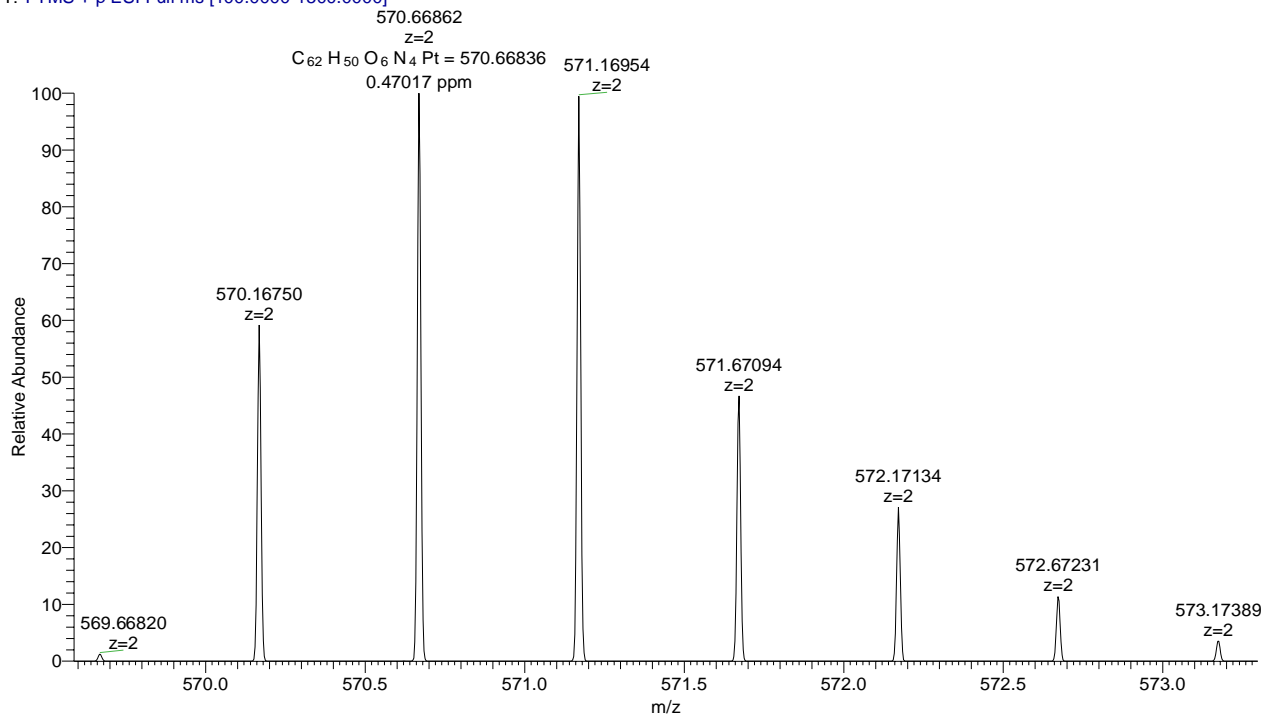
Theoretical isotope pattern of $[\text{C}_{70}\text{H}_{66}\text{N}_4\text{O}_6\text{Pt}]^{2+}$

C70H64N4O6Pt +H: C70 H66 N4 O6 Pt1 p(gss, s/p:40) Ch...



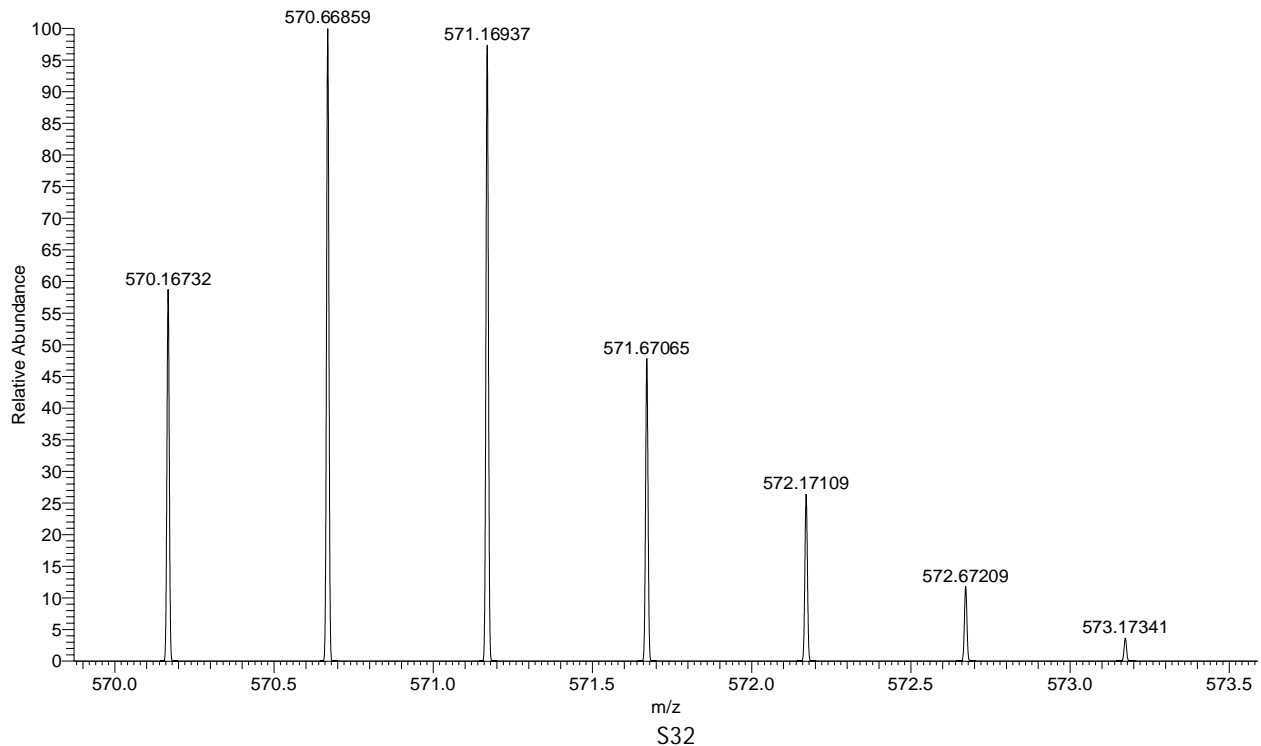
(e) [5+2H]²⁺

zhaoshunan-20220929-5 #11-27 RT: 0.05-0.12 AV: 17 NL: 3.06E8
 T: FTMS + p ESI Full ms [100.0000-1500.0000]



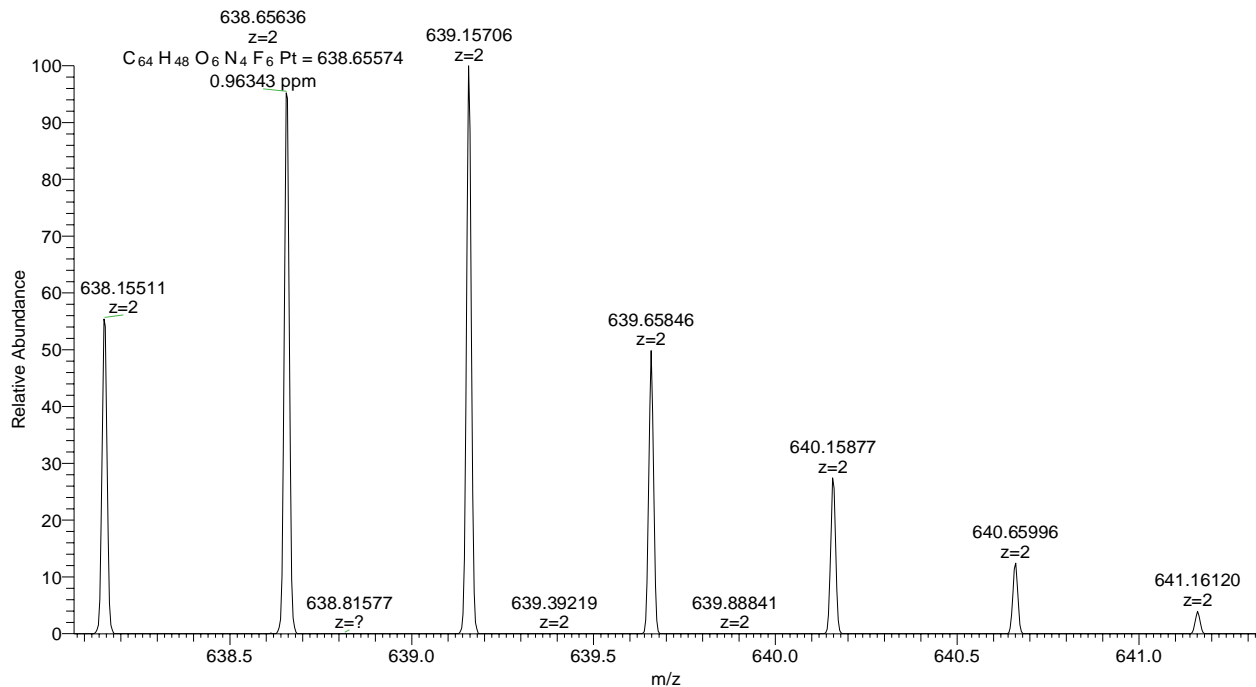
Theoretical isotope pattern of [C₆₂H₅₀N₄O₆Pt]²⁺

C62H48N4O6Pt +H: C62 H50 N4 O6 Pt1 p(gss, s/p:40) Ch...



(f) [6+2H]²⁺

zhaoshunan-20220929-6 #9-27 RT: 0.04-0.12 AV: 19 NL: 2.46E8
T: FTMS + p ESI Full ms [100.0000-1500.0000]



Theoretical isotope pattern of $[C_{64}H_{48}F_6N_4O_6Pt]^{2+}$

C64H46F6N4O6Pt +H: C64 H48 F6 N4 O6 Pt1 p(gss, s/p:4...

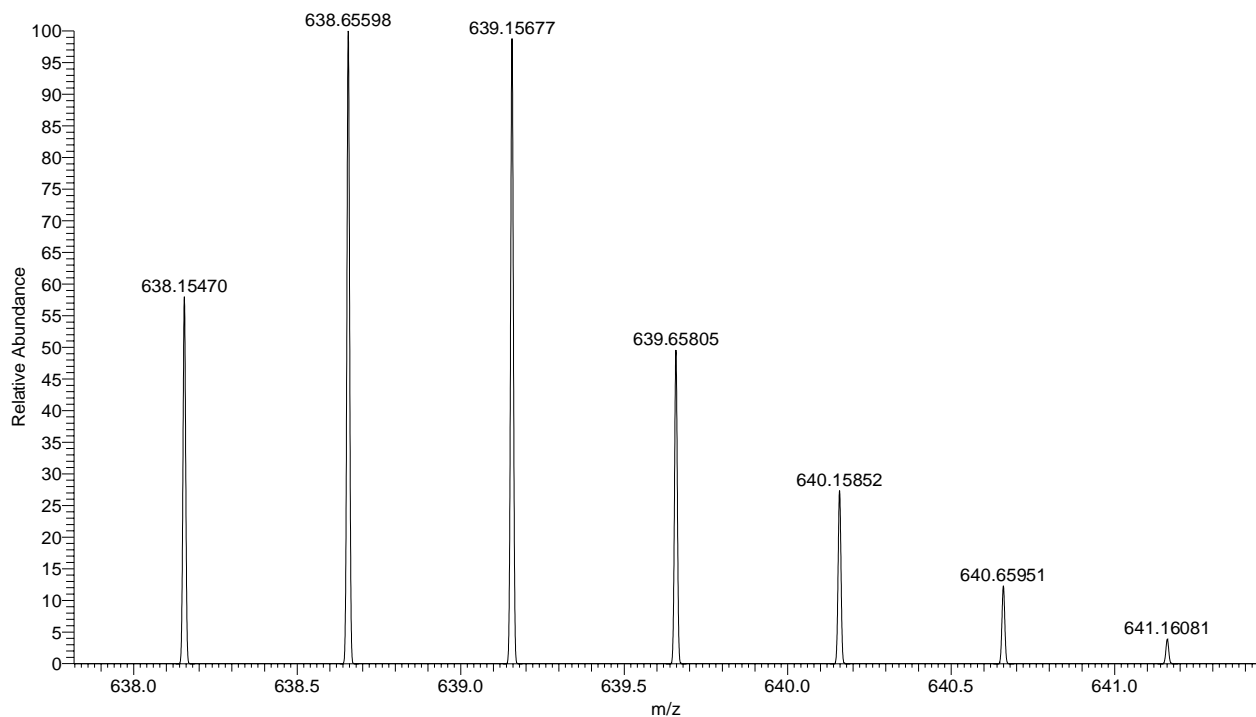


Figure S13. High-resolution mass spectra (up) and the corresponding simulated isotope patterns (down) of 1–6 (a–f).

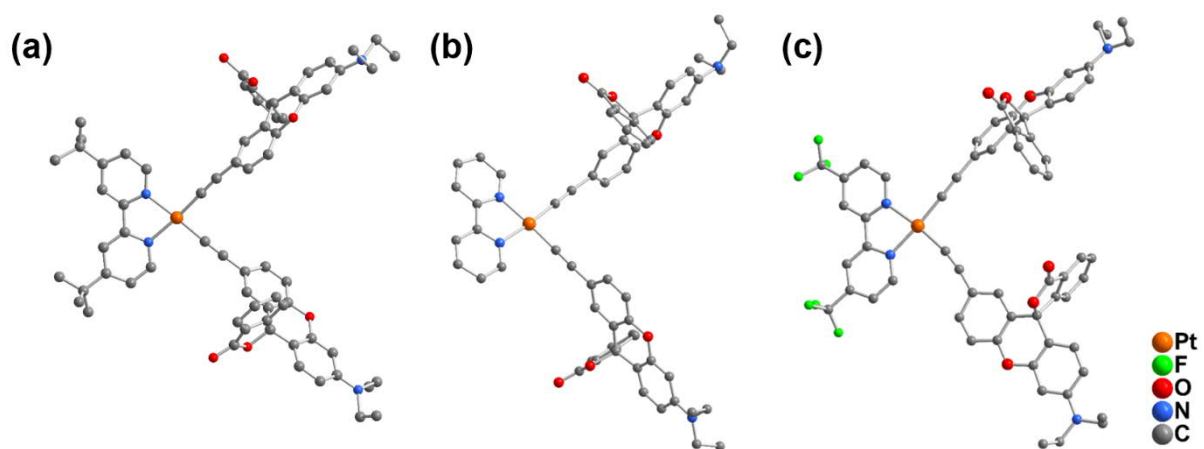


Figure S14 Ball-and-stick model showing the crystal structures of **4** (a), **5** (b) and **6** (c).

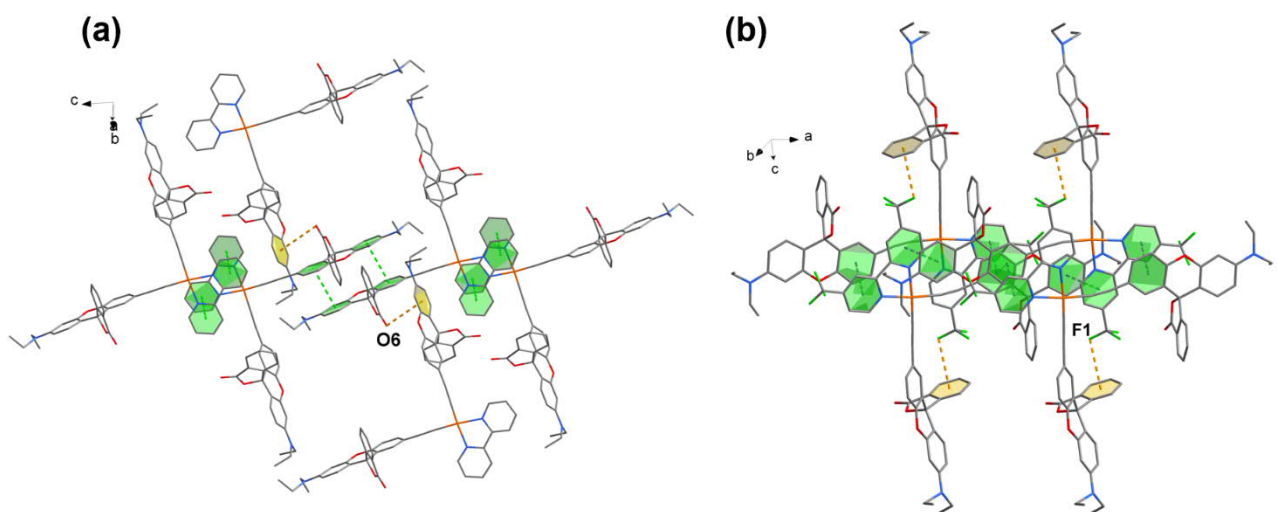


Figure S15. Wires-or-sticks model showing the π - π stacking interactions (green rings and green spot lines) of **5** (a), **6** (b), and the O... π interactions (yellow rings and yellow spot lines) for **5**, F... π interactions (yellow rings and yellow spot lines) for **6**.

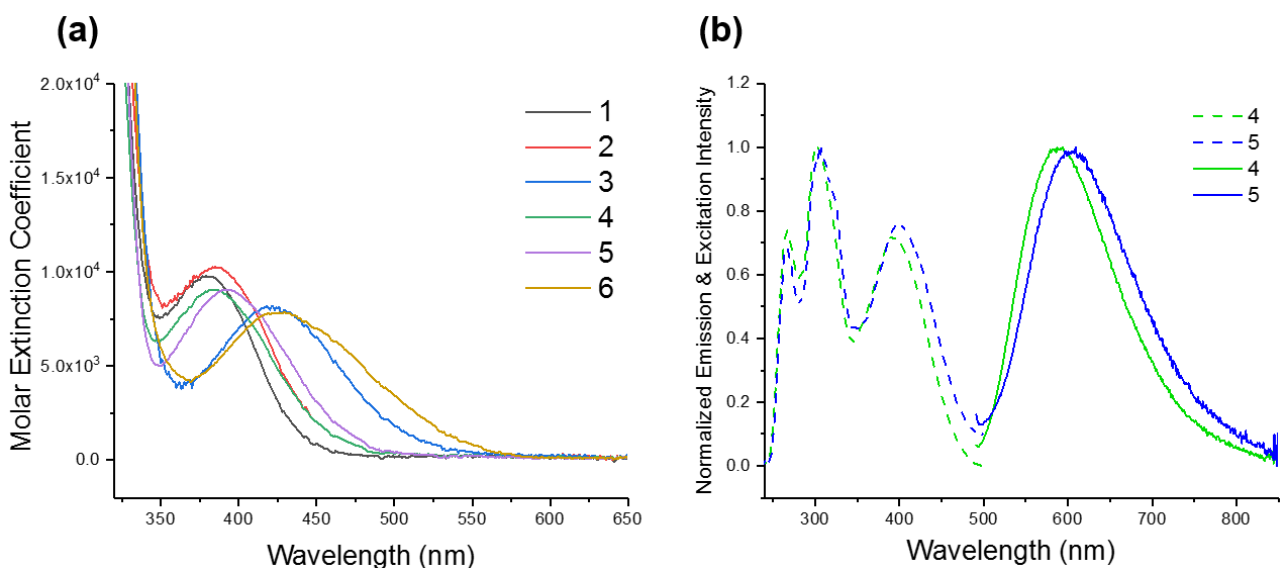


Figure S16. (a) Molar Extinction Coefficient spectra of **1-6** in acetonitrile at room temperature; (b) Normalized emission (solid lines, $\lambda_{ex} = 355$ nm) and excitation (dash lines) spectra of **4**, **5**. Deoxygenated samples were prepared for emission measurement.

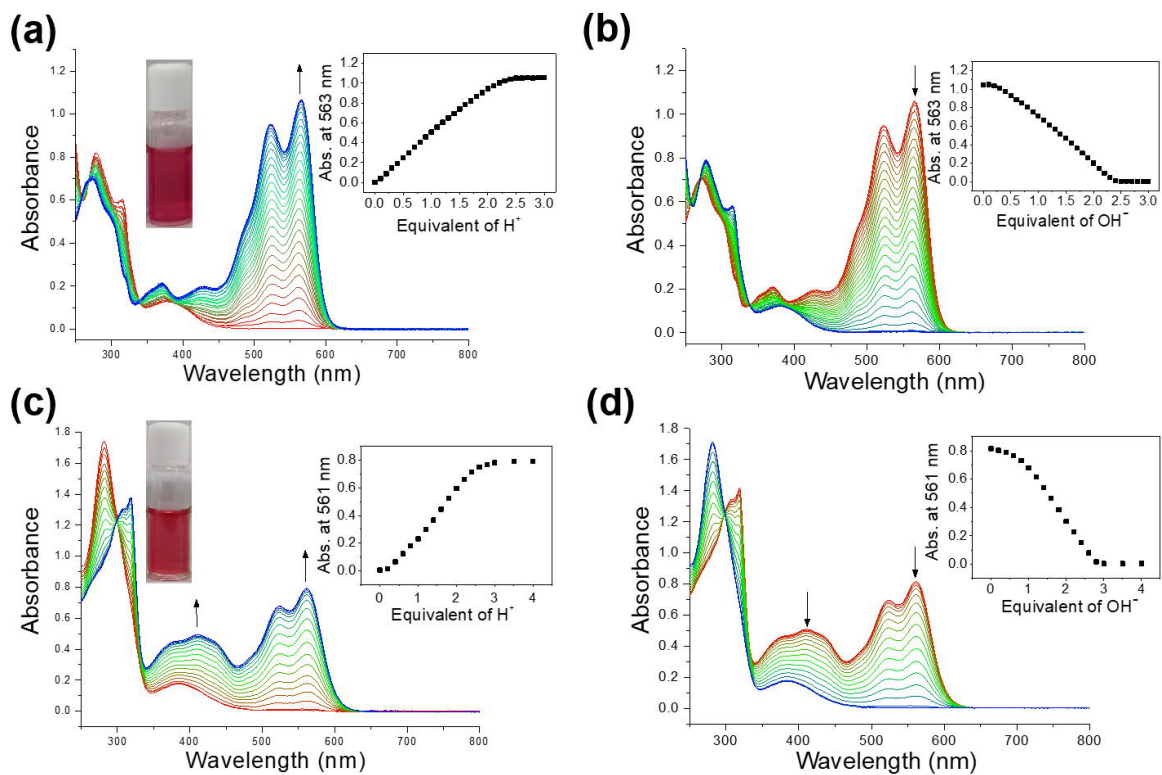


Figure S17. The electronic absorption spectral changes of (a, b) **1** (conc. = 2×10⁻⁵ M) and (c, d) **4** (conc. = 2×10⁻⁵ M) upon the addition of various equivalents of acid (a, c) and base (b, d) in acetonitrile at room temperature. The insets show plots of absorbance versus the concentration of protons and OH⁻, photos of the solution colors in the opened forms.

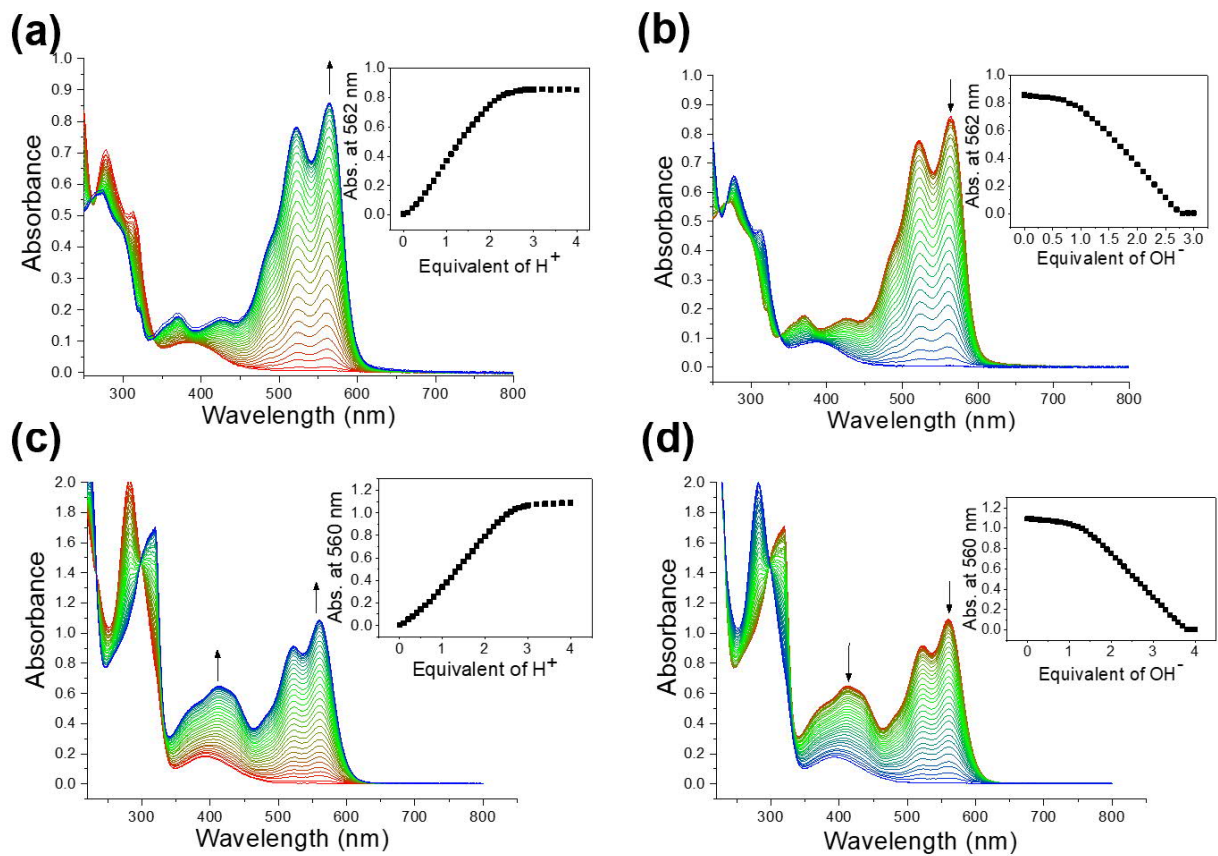


Figure S18. The electronic absorption spectral changes of (a, b) **2** (conc. = 2×10^{-5} M) and (c, d) **5** (conc. = 2×10^{-5} M) upon the addition of various equivalents of protons (a, c) and base (b, d) in acetonitrile at room temperature. The insets show plots of absorbance versus the concentration of protons and the solution colors in the opened forms.

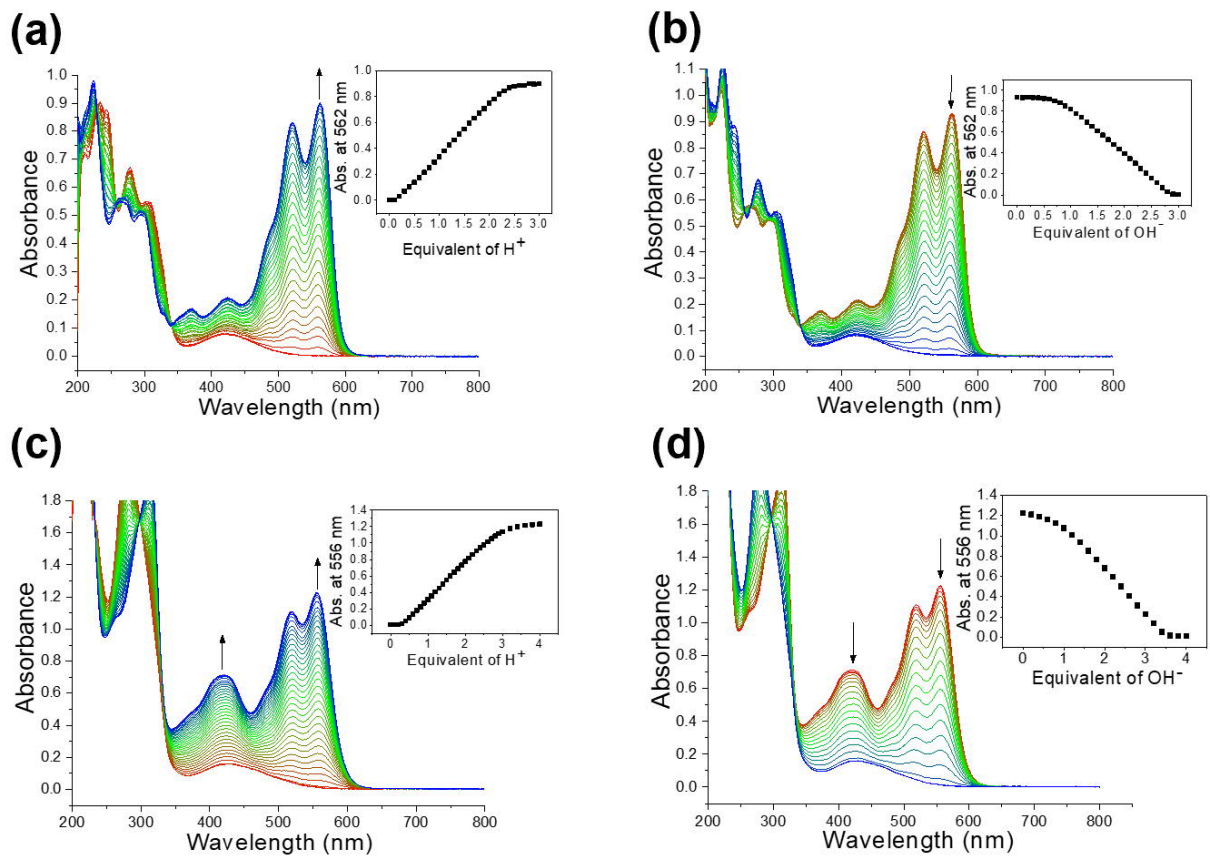


Figure S19. The electronic absorption spectral changes of (a, b) **3** (conc. = 2×10^{-5} M) and (c, d) **6** (conc. = 2×10^{-5} M) upon the addition of various equivalents of protons (a, c) and base (b, d) in acetonitrile at room temperature. The insets show plots of absorbance versus the concentration of protons and the solution colors in the opened forms.

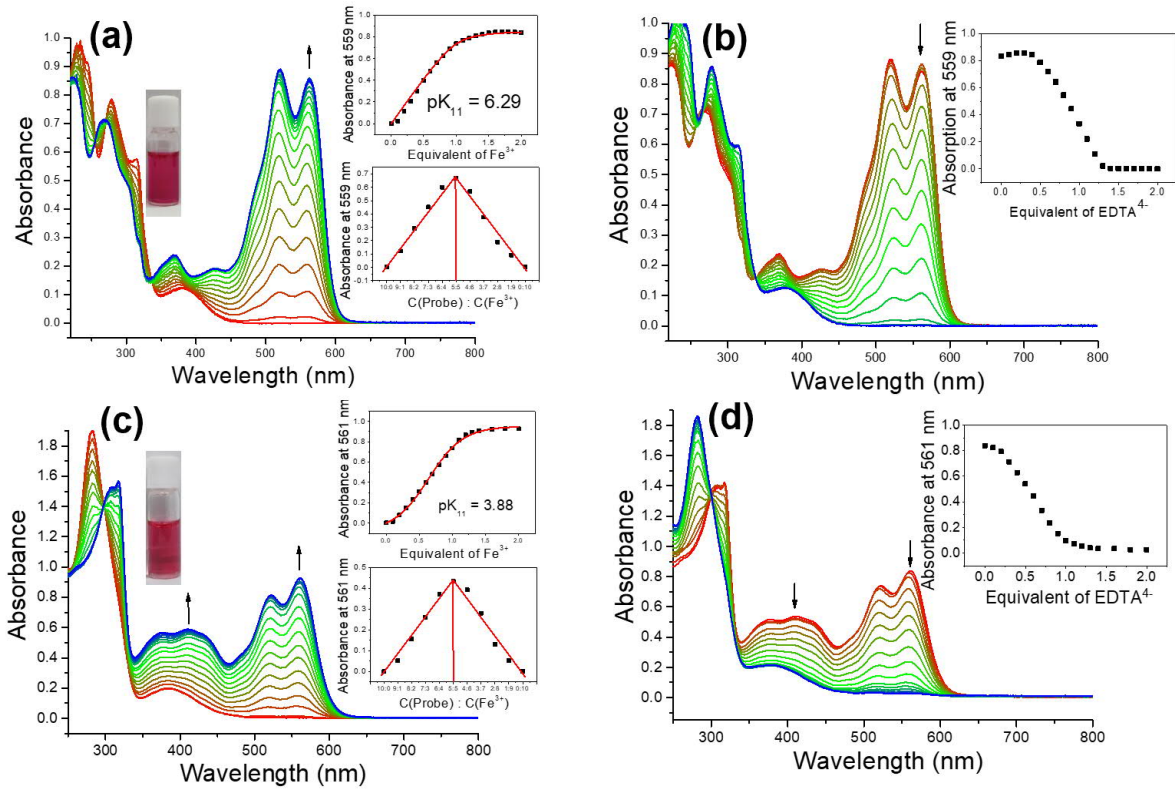


Figure S20. The electronic absorption spectral changes of (a, b) **1** (conc. = 2×10^{-5} M) and (c, d) **4** (conc. = 2×10^{-5} M) upon the addition of various equivalents of Fe(III) (a, c) and EDTA (b, d) in acetonitrile at room temperature. The insets show plots of absorbance versus the concentration of Fe(III) and EDTA, photos of the solution colors in the opened forms.

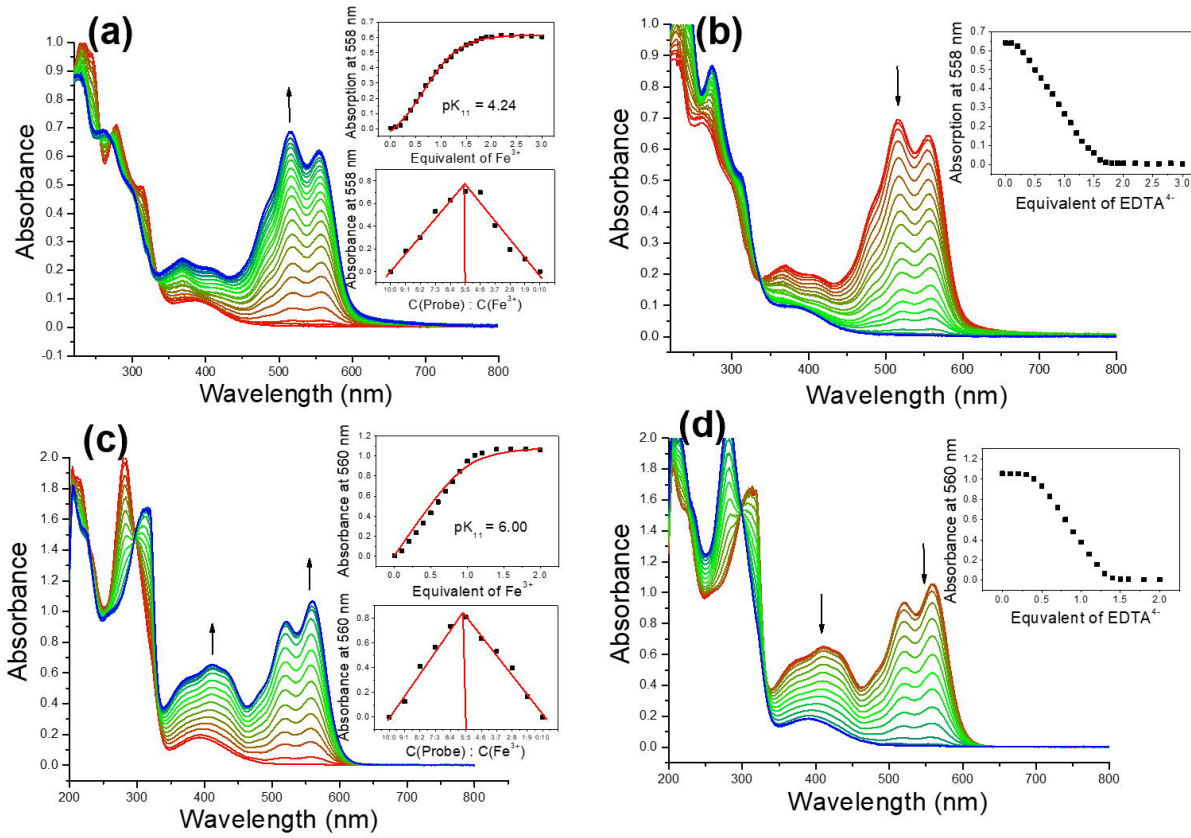


Figure S21. The electronic absorption spectral changes of (a, b) **2** (conc. = 2×10^{-5} M) and (c, d) **5** (conc. = 2×10^{-5} M) upon the addition of various equivalents of Fe(III) (a, c) and EDTA (b, d) in acetonitrile at room temperature. The insets show plots of absorbance versus the concentration of Fe(III) and EDTA.

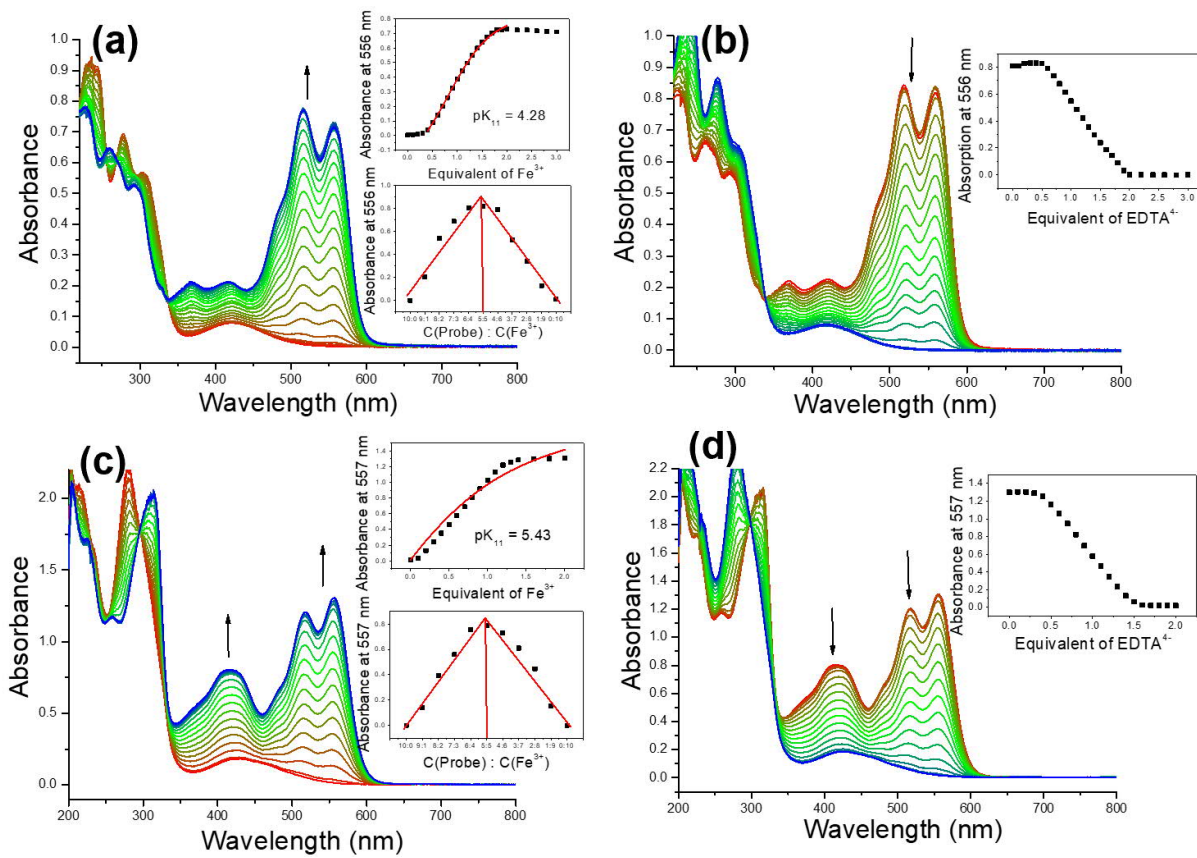


Figure S22. The electronic absorption spectral changes of (a, b) **3** (conc. = 2×10^{-5} M) and (c, d) **6** (conc. = 2×10^{-5} M) upon the addition of various equivalents of $\text{Fe}(\text{III})$ (a, c) and EDTA (b, d) in acetonitrile at room temperature. The insets show plots of absorbance versus the concentration of $\text{Fe}(\text{III})$ and EDTA .

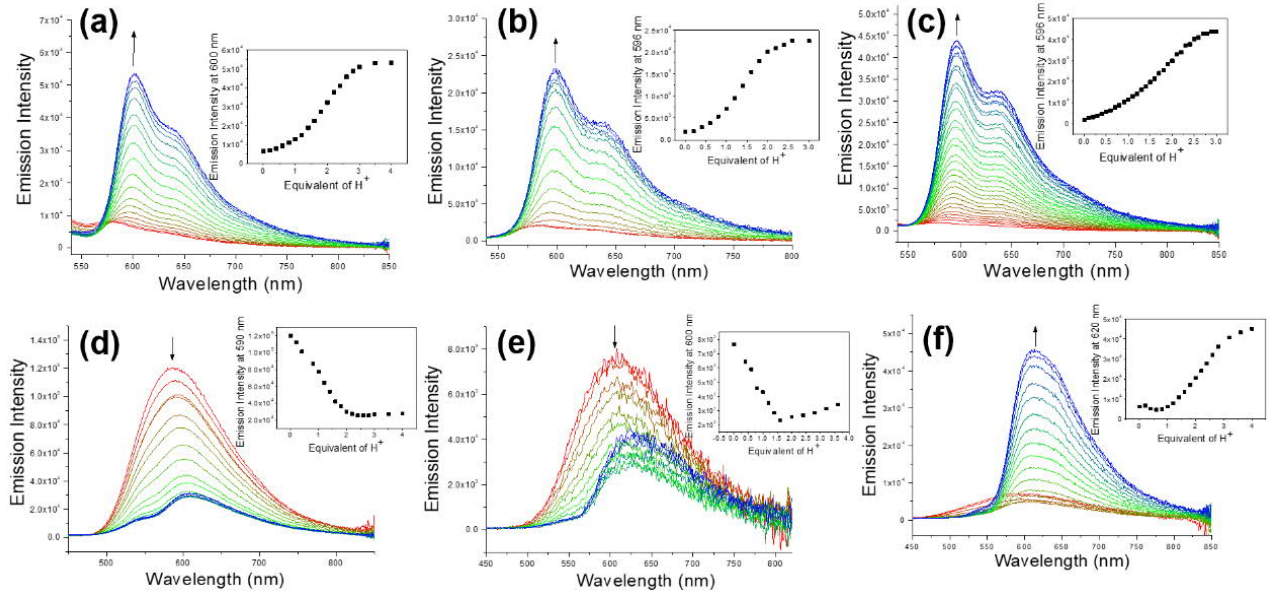


Figure S23. Emission spectra for **1** (a), **2** (b), **3** (c), **4** (d), **5** (e), **6** (f) by adding acid gradually with the excitation wavelength of the isosbestic points.

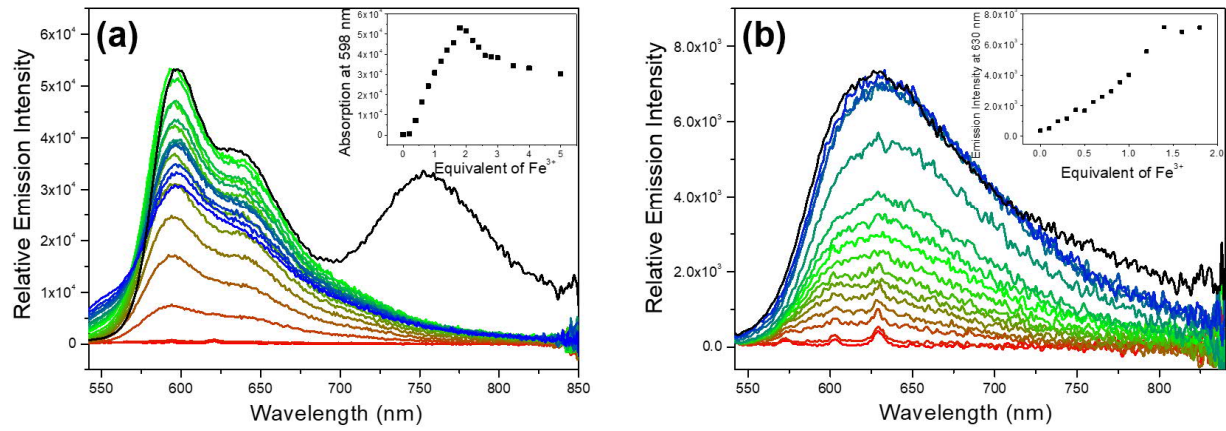


Figure S24. Emission spectral changes in acetonitrile upon the addition of various concentrations of Fe(III) ions to (a) **2** and (b) **5** at an excitation wavelength of 532 nm; conc. = 2×10^{-5} M. The inserts show plots of the relative emission intensity versus the equivalents of Fe(III) ions. Black line: deoxygenated solution with an excess of Fe(III) ions.

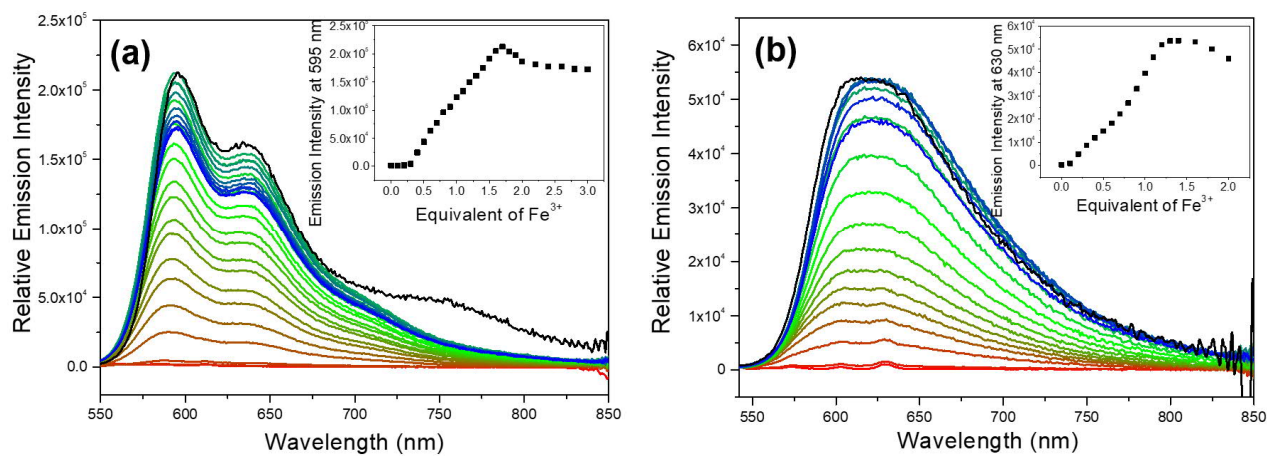


Figure S25. Emission spectral changes in acetonitrile upon the addition of various concentrations of Fe(III) ions to (a) **3** and (b) **6** at an excitation wavelength of 532 nm; conc. = 2×10^{-5} M. The inserts show plots of the relative emission intensity versus the equivalents of Fe(III) ions. Black line: deoxygenated solution with an excess of Fe(III) ions.

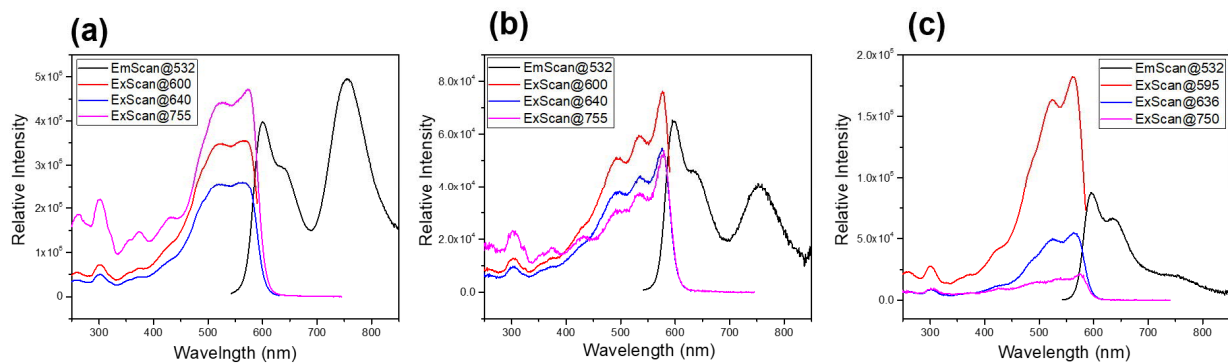


Figure S26. Excitation spectra of opened form of **1** (a) monitored at 600 nm, 640 nm and 755 nm, **2** (b) at 600 nm, 640 nm and 755 nm, **3** (c) at 595 nm, 636 nm and 750 nm in their ring-opened form triggered by Fe(III) ion in acetonitrile.

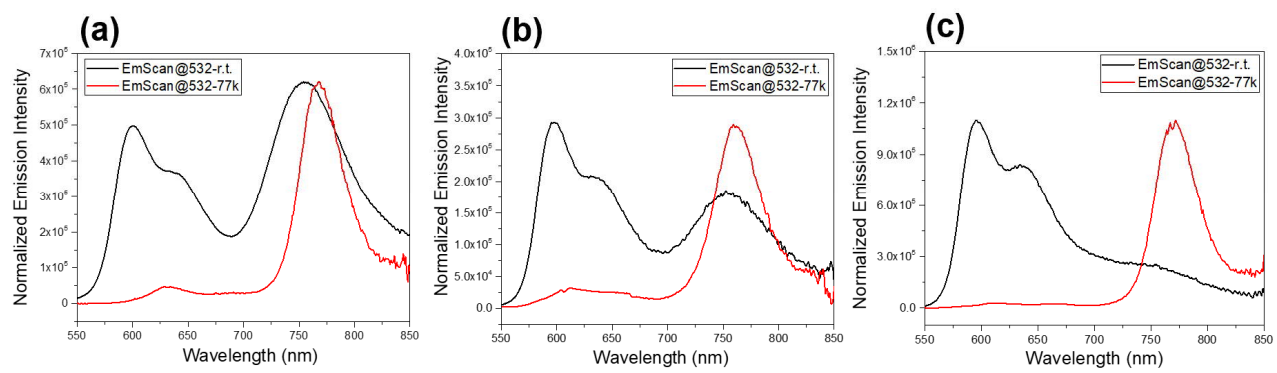


Figure S27. Normalized emission spectra for **1** (a), **2** (b) and **3** (c) with 532 nm excitation under room temperature (r. t.) and 77 k.

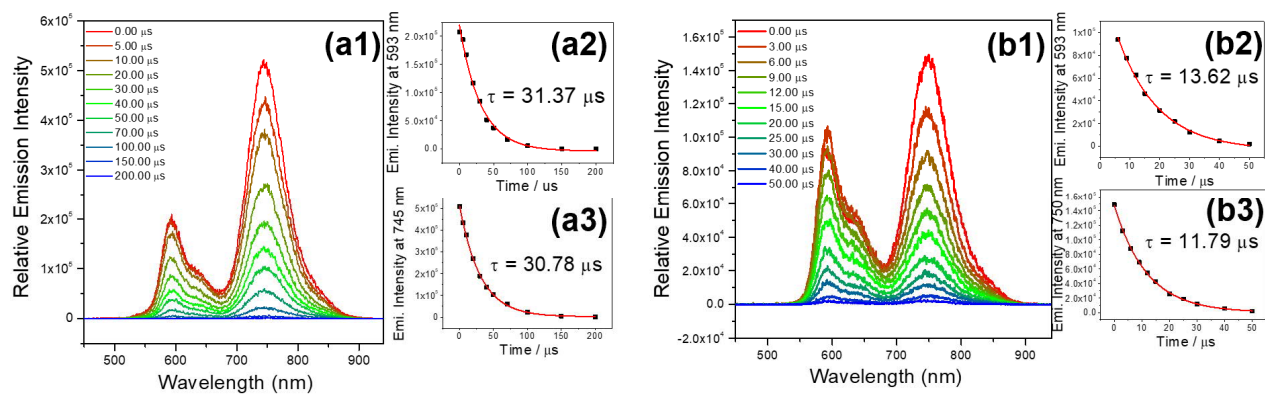


Figure S28. Time-resolved emission spectra of **2** (a1) and **3** (b1) in the ring-opened form in deoxygenated acetonitrile at room temperature and the corresponding lifetime decay traces monitored at 593 nm (with the exclusion of the first data point) (a2) and 745 nm (a3) for **2**, 593 nm (with the exclusion of the first data point) (b2) and 750 nm (b3) for **3**. Conc. = 2×10^{-5} M and 3 equivalents of Fe(III) ions. A pulsed laser at 532 nm was the excitation source.

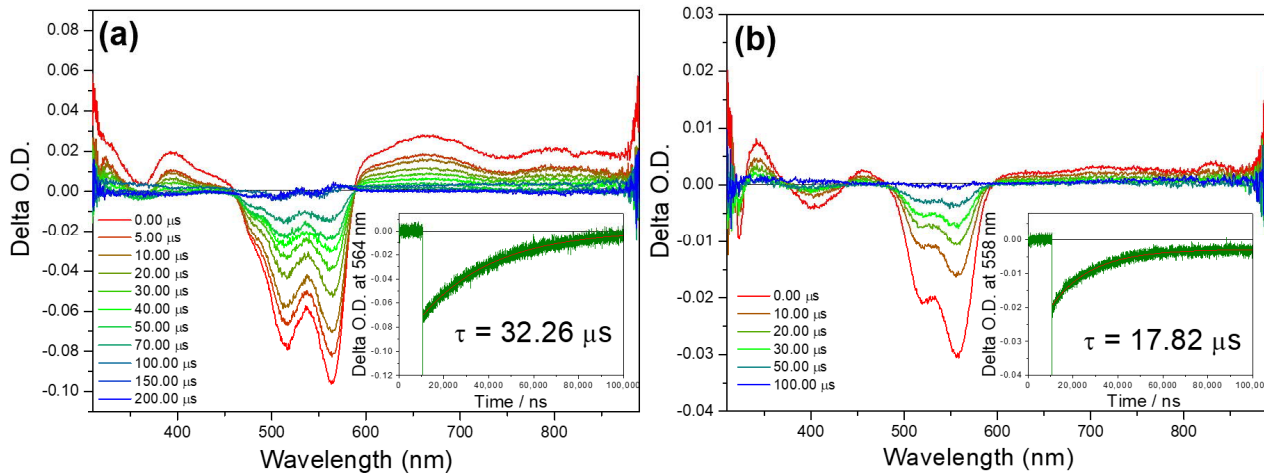


Figure S29. Transient absorption spectral changes of (a) **2** (conc. = 2×10^{-5} M) and (b) **5** (conc. = 2×10^{-5} M) in their ring-opened forms with 3 equivalent of Fe(III) ions in deoxygenated acetonitrile at room temperature. The insets show the transient absorption lifetime fitting of the signals monitored at 564 nm and 558 nm for **2** and **5**, respectively. Excitation wavelength = 355 nm.

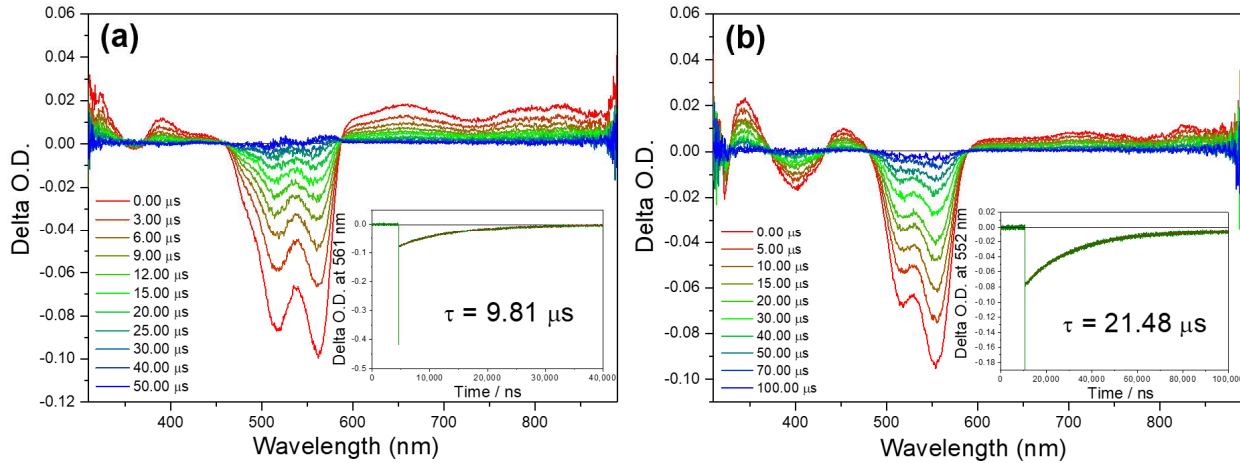


Figure S30. Transient absorption spectral changes of (a) **3** (conc. = 2×10^{-5} M) and (b) **6** (conc. = 2×10^{-5} M) in their ring-opened forms with 3 equivalent of Fe(III) ions in deoxygenated acetonitrile at room temperature. The inserts show the transient absorption lifetime fitting of the signals monitored at 561 nm and 552 nm for **3** and **6**, respectively. Excitation wavelength = 355 nm.

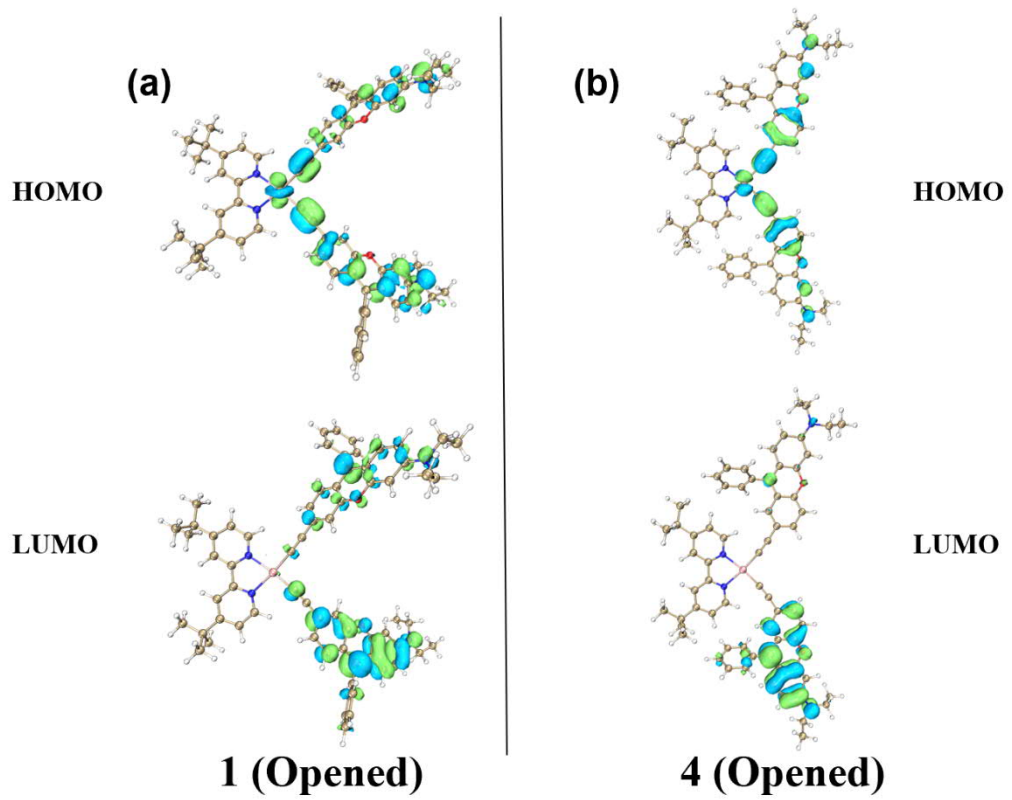


Figure S31. The electronic density distribution of the HOMO and LUMO opened form of **1** and **4**.

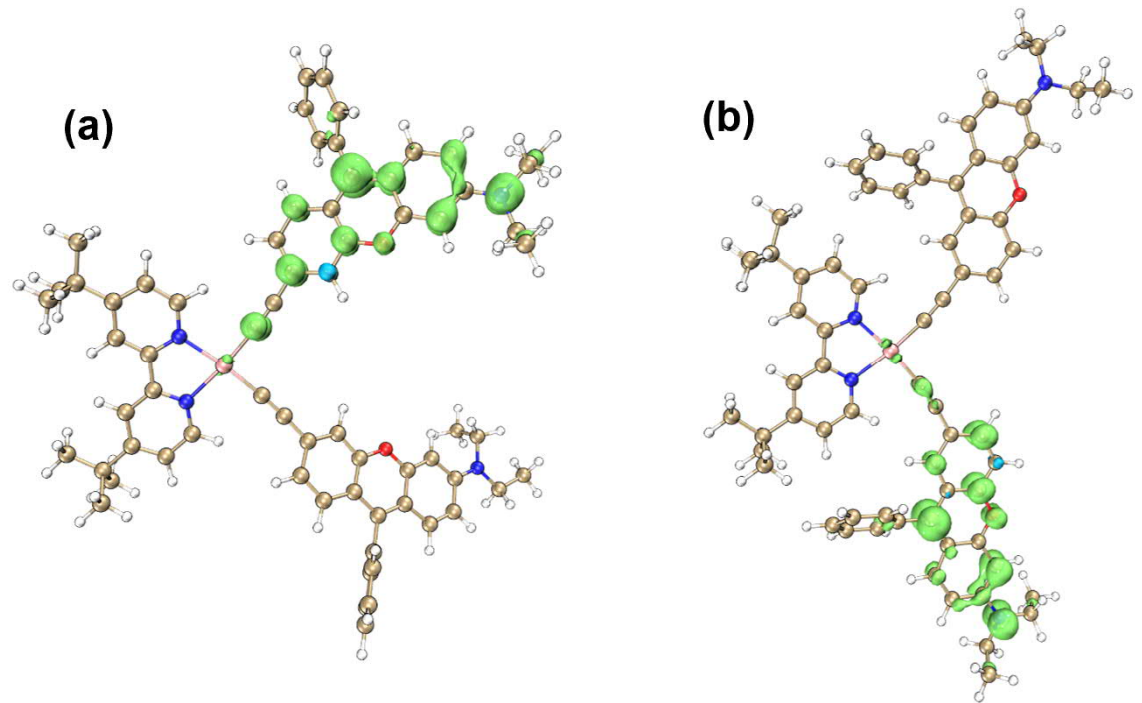


Figure S32. The spin density of the opened form for **1** (a) and **4** (b).

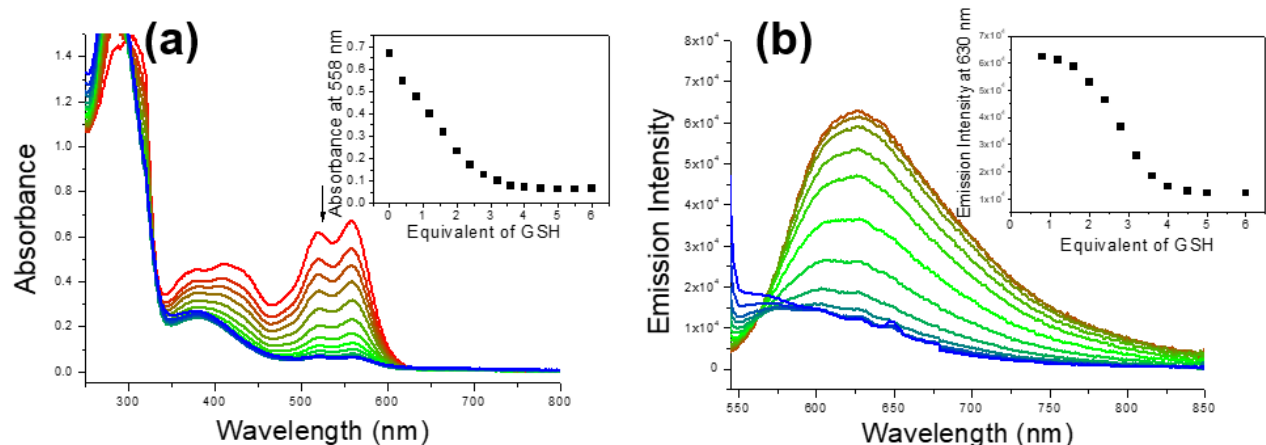


Figure S33. The absorption and emission spectral of **4** (a, b) (conc. = 2×10^{-5} M) with 3 equivalent of Fe(III) ions upon the addition of various equivalents of GSH (aqua. solution) in acetonitrile at room temperature. The insets show plots of absorbance versus the concentration of GSH.

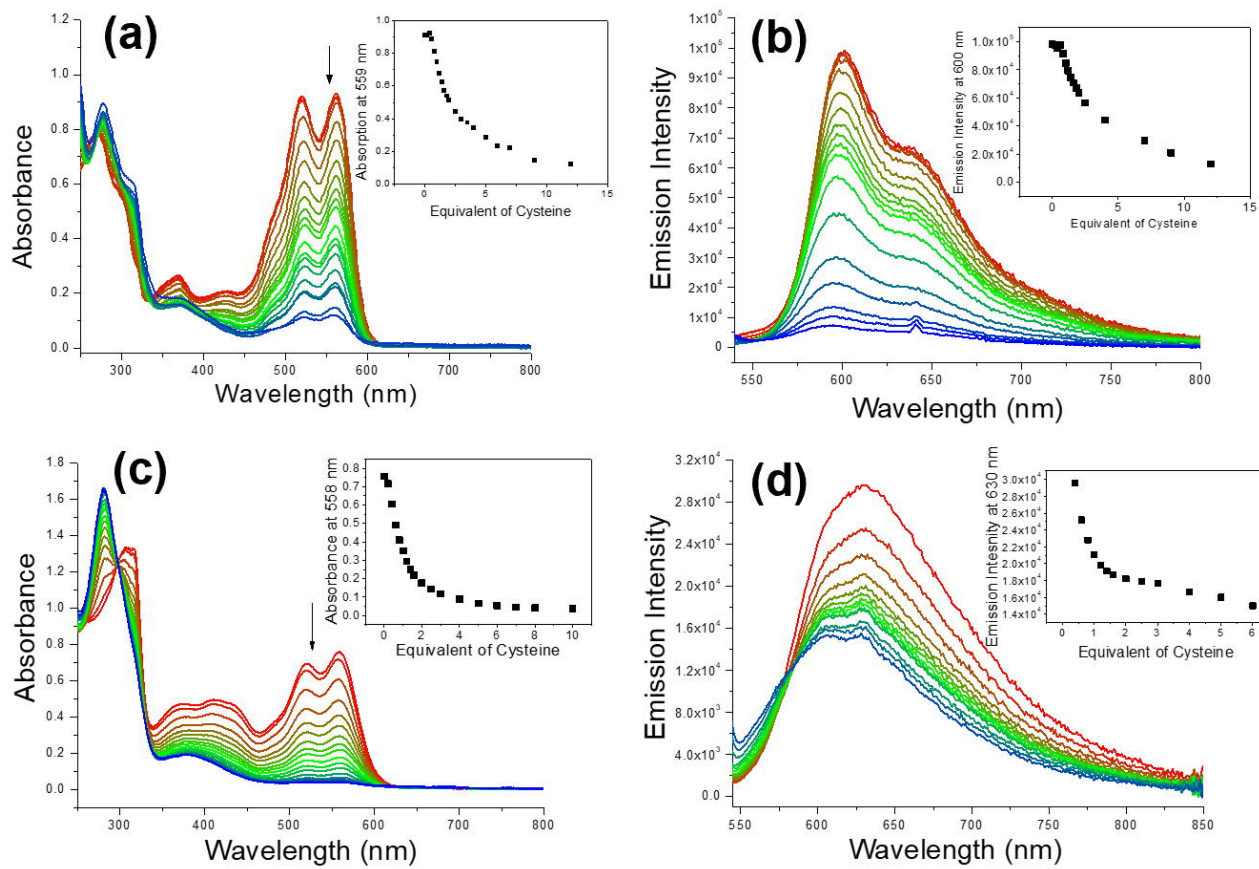


Figure S34. The absorption and emission spectral of **1** (a, b) and **4** (c, d) (conc. = 2×10^{-5} M) with 3 equivalent of Fe(III) upon the addition of various equivalents of Cysteine (aqua. solution) in acetonitrile at room temperature. The insets show plots of absorbance versus the concentration of Cysteine.

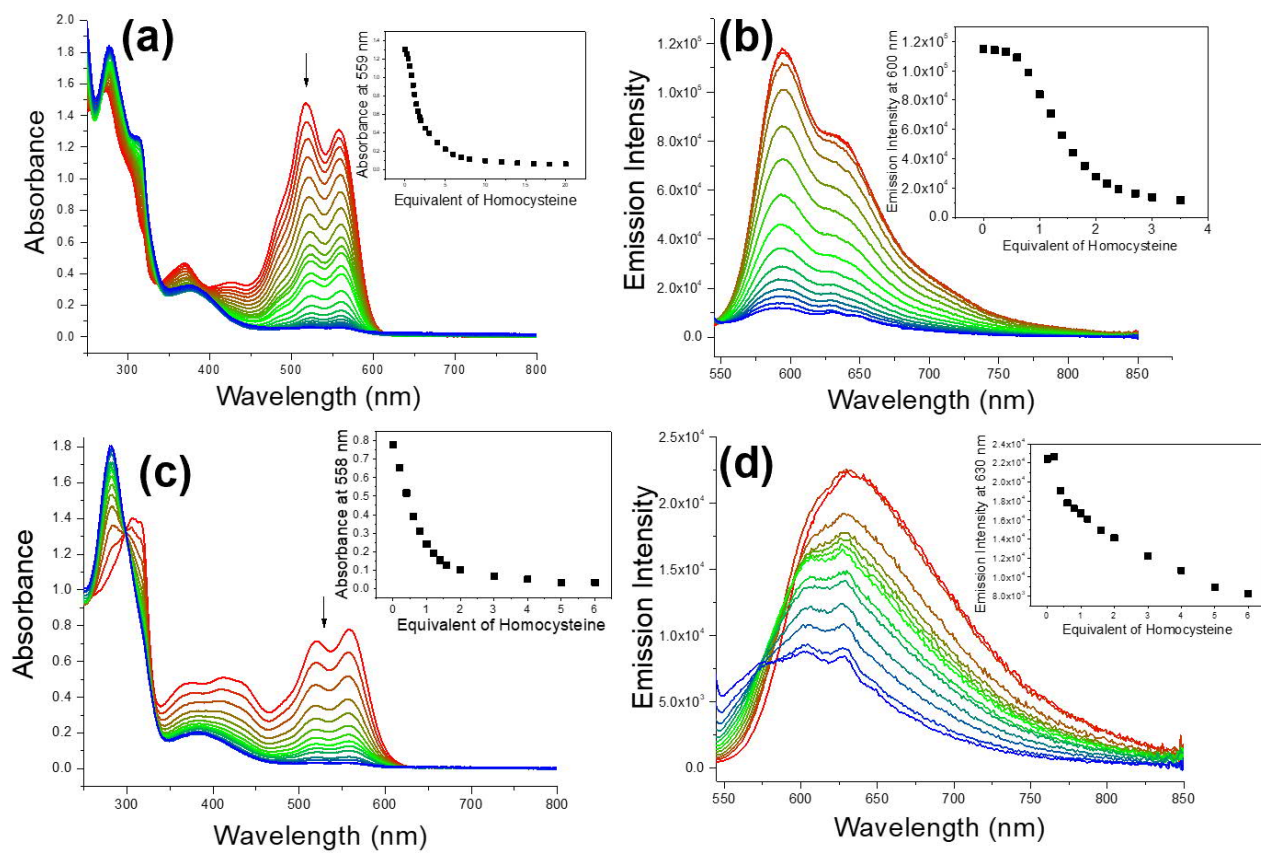


Figure S35. The absorption and emission spectral of **1** (a, b) and **4** (c, d) (conc. = 2×10^{-5} M) with 3 equivalent of Fe(III) upon the addition of various equivalents of Homocysteine (aqua. solution) in acetonitrile at room temperature. The insets show plots of absorbance versus the concentration of Homocysteine.

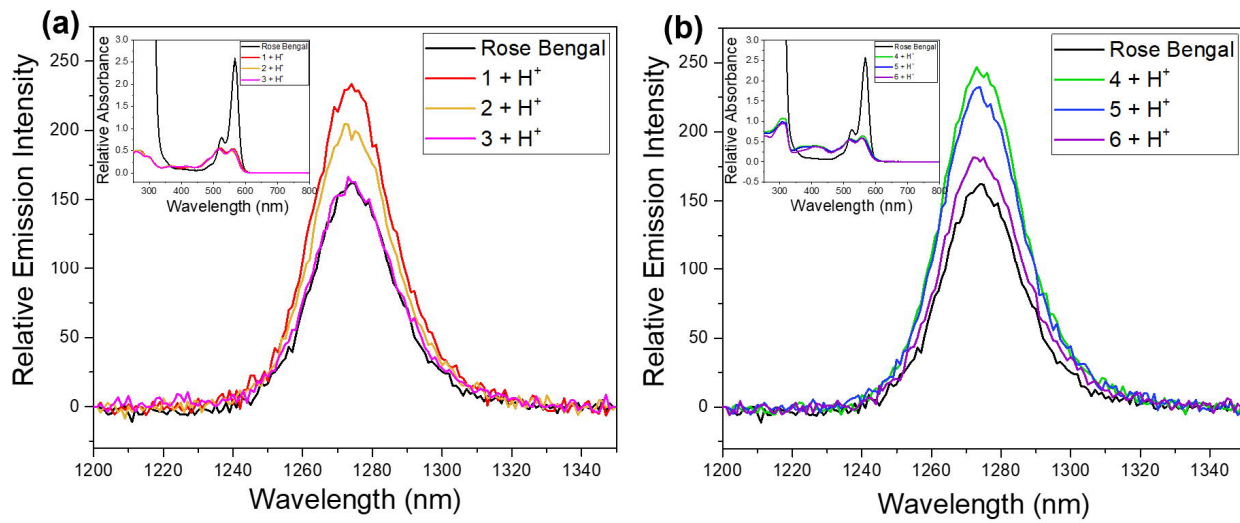


Figure S36. Singlet oxygen emission spectra of **1–3** (a) and **4–6** (b) with excess amount of acid in acetonitrile, Rose Bengal as the reference agent. Insets show the corresponding absorption spectra in the measurement.

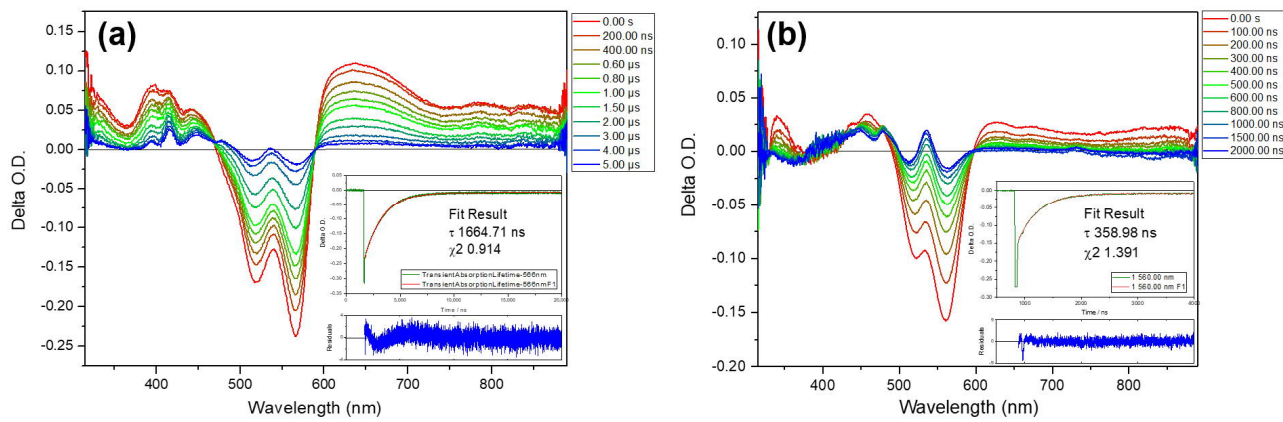
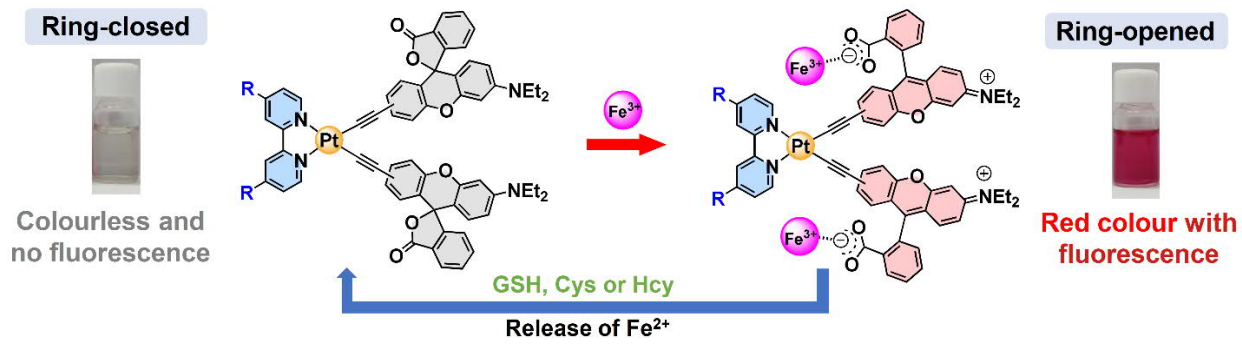


Figure S37. Transient absorption spectral of **1** (a) and **4** (b) with 5 equivalents of acid upon the addition of 10 equivalents of perylene in acetonitrile at room temperature. Inserts are the lifetime of bleaching bands. $\lambda_{\text{ex}} = 532 \text{ nm}$.



Scheme S2 Schematic illustration of chemo-induced irreversible ring-opening and closing processes for **1–6** with the optical responses of acid or $\text{Fe}(\text{III})$ ion.

Reference

- S1 Y. Ai, M. Ng, E. Y. Hong, A. K. Chan, Z. W. Wei, Y. Li and V. W. Yam, *Chemistry*, 2018, **24**, 11611-11618.
- S2 S. Zhao, Y. Zhu, L. Li, V. Guerchais, J. Boixel and K. M. C. Wong, *Chem. Sci.*, 2021, **12**, 11056-11064.
- S3 T. N. Singh-Rachford and F. N. Castellano, *Coordination Chemistry Reviews*, 2010, **254**, 2560-2573.
- S4 R. R. Islangulov, J. Lott, C. Weder and F. N. Castellano, *J. Am. Chem. Soc.* 2007, **129**, 12652-12653.
- S5 F. Stracke, M. Heupel and E. Thiel, *J. Photochem. Photobiol. Chem.*, 1999, **126**, 51–58.
- S6 G. M. Sheldrick, *Acta Crystallogr. A*, 2008, **64**, 112-122.
- S7 G. M. Sheldrick, SHELXL-97: Program for Crystal Structure Solution and Refinement; University of Göttingen: Göttingen, Germany, 1997.
- S8 A. D. Becke, *The Journal of Chemical Physics.*, 1993, **98**, 5648-5652.
- S9 J. P. Perdew and Y. Wang, *Phys. Rev. B Condens. Matter.*, 1992, **45**, 13244-13249.
- S10 S. Grimme, S. Ehrlich and L. Goerigk, *J. Comput. Chem.*, 2011, **32**, 1456-1465.
- S11 S. Grimme, J. Antony, S. Ehrlich and H. Krieg, *J Chem Phys.*, 2010, **132**, 154104.
- S12 F. Neese, *WIREs Computational Molecular Science*, 2011, **2**, 73-78.
- S13 T. Lu, F. Chen, *J. Comput. Chem.*, 2012, **33**, 580-592.
- S13 W. Humphrey, A. Dalke and K. Schulten, *J Mol Graph.*, 1996, **14**, 33-38.